

This document is the Accepted Manuscript version of a Published Work that appeared in final form in The Journal of Physical Chemistry C, copyright © American Chemical Society after peer review and technical editing by the publisher. To access the final edited and published work see <https://pubs.acs.org/articlesonrequest/AOR-nMBBFIC9thwW5nbXCVvh>.

Self-Assembled Monolayers with Distributed Dipole Moments Originating from Bipyrimidine Units

Michael Gärtner,^{†,#} Eric Sauter,^{‡,#} Giulia Nascimbeni,^{1,#} Adrian Wiesner,[†] Martin Kind,[†] Philipp Werner,[†] Christian Schuch,[†] Tarek Abu-Husein,[†] Andika Asyuda,[‡] Jan W. Bats,[§] Michael Bolte,[†] Egbert Zojer,^{1,*} Andreas Terfort,^{†,*} and Michael Zharnikov^{‡,*}

[†]*Institut für Anorganische und Analytische Chemie, Johann Wolfgang Goethe Universität Frankfurt, Max-von-Laue-Straße 7, D-60438 Frankfurt am Main, Germany*

[‡]*Angewandte Physikalische Chemie, Universität Heidelberg, Im Neuenheimer Feld 253, D-69120 Heidelberg, Germany*

¹*Institute of Solid State Physics, Graz University of Technology, Petersgasse 16, 8010 Graz, Austria*

[§]*Institute of Organic Chemistry and Chemical Biology, Johann Wolfgang Goethe Universität Frankfurt, Max-von-Laue-Straße 7, D-60438 Frankfurt am Main, Germany*

these authors have provided equivalent contributions

Abstract

The concept of distributed dipoles in monomolecular self-assembly on solid substrates was tested for the example of thiolate self-assembled monolayers (SAMs) on Au(111) containing dipolar 2,5'-bipyrimidine units. These were attached to a thiol anchoring group either directly or via a phenylene-methylene spacer, with the spacer decoupling the dipolar moiety from the substrate and promoting layer formation. As expected, the SAMs containing spacer groups exhibited a higher quality, including a higher packing density and nearly upright molecular orientation. The electrostatic effects of the dipolar bipyrimidine moieties were tested through C 1s and N 1s photoemission spectra, where electrostatic core-level shifts impact the shapes of the spectra. Additionally, changing the orientation of the dipoles allows a variation of the work function over a range of ~ 1.35 eV. The experiments were complemented by density-functional theory calculations. The work function tuning range was reasonably high, but smaller than expected considering that for SAMs with a single embedded pyrimidine group per molecule work-function changes already amounted to ~ 1.0 eV. This behavior is rooted in an asymmetry of the studied SAMs: For dipoles pointing away from the substrate, the expected doubling of the work function change between monopyrimidine and bipyrimidine SAMs essentially occurs. Conversely, for the downward-oriented pyrimidine dipoles, the second polar ring has hardly any effect. Consistent observations were made for the core-level shifts. We discuss several factors, which are potentially responsible for this asymmetry, like disorder, depolarization, or Fermi-level pinning. Of these, the most likely explanation is the adsorption of airborne contaminants interacting with the nitrogen atoms in the immediate vicinity of the outer surface, which are present only in films with downward oriented dipoles. In spite of these complications, some of the introduced distributed dipole SAMs serve as important model systems for understanding electrostatic effects at interfaces. They are also of interest for controlling carrier-injection barriers in organic (opto)electronic devices.

1. Introduction

The performance of organic electronic and photovoltaic devices depends to a large extent on the control over the injection barriers and the energy-level alignments between adjacent layers.^{1,2} In many cases, these quantities can be optimized by interfacial dipole engineering employing suitable dipolar self-assembled monolayers (SAMs), specifically adjusted to a particular substrate or interface.³⁻⁷ The adjustment occurs by selecting a proper docking group, providing the bonding to the substrate in a predefined orientation.⁸ An example would be thiolates in the case of gold, which is a popular electrode material especially for transistors. The backbones of the SAM constituents then have a nearly upright orientation, exposing their terminal groups to the SAM-ambient interface. The molecular alignment resulting from such an architecture also orients polar functional groups incorporated into the molecules. Depending on the orientation of these polar groups, their density, and dipole moment, the work function of the resulting interface can be adjusted to specific requirements.

In most cases, a polar moieties are introduced as terminal tail groups, changing, simultaneously, the electronic and the chemical character of the SAM-ambient interface. Frequently used moieties in this context are the $-F$, $-CF_3$, $-CN$, $-NH_2$, $-NO_2$, and $-CH_3$ groups.^{4,9-11} Alternatively, a polar moiety can be embedded into the molecular backbone, which allows work function engineering without changing the chemical character of the SAM-substrate and SAM-ambient interfaces.¹²⁻¹⁵ In this way, the electrostatic and chemical properties of the SAM can be decoupled. Of particular interest in this context are SAMs with an embedded pyrimidine group, which (depending on the orientation of the dipoles) are able to change the work functions of Au(111) and Ag(111) substrates over a range of ~ 1 eV and ~ 0.85 eV, respectively.^{13,15-17} Optimized pyrimidine-substituted monolayers have also been successfully used for minimizing contact resistances in p-type and n-type organic thin film transistors and distinctly improved the performance of more complex electronic circuits on flexible substrates.¹⁸ These highly promising properties of pyrimidine groups as embedded dipoles raises the question, whether even better results could be obtained by including more than one such unit into a single molecule. The simplest structural unit to be incorporated into such a distributed dipole SAM¹⁹ is bipyrimidine.²⁰⁻²²

Accordingly, we present here two series of SAMs containing bipyrimidine units with both pyrimidine groups oriented in parallel. In the first system, the bipyrimidine unit is directly attached to a thiol docking group (PmPm-up/down), while in the second system it is separated from it by a phenylene-methylene spacer (PmPmP1-up/down, Figure 1). The latter decouples

the bipyrimidine moiety from the substrate and, additionally, promotes the molecular assembly.²³ The advantage of the PmPm-up/down systems for modifying injection barriers at electrodes is that they should give rise to much shorter tunneling barriers compared to their PmPmP1-up/down analogues due to their smaller molecular length.^{15,18} The thiol docking group used in both systems enables the bonding to coinage metal substrates including Au(111). The latter was selected by us in the present case since it is frequently used as model substrate in fundamental SAM studies and as electrode material in organic transistors.

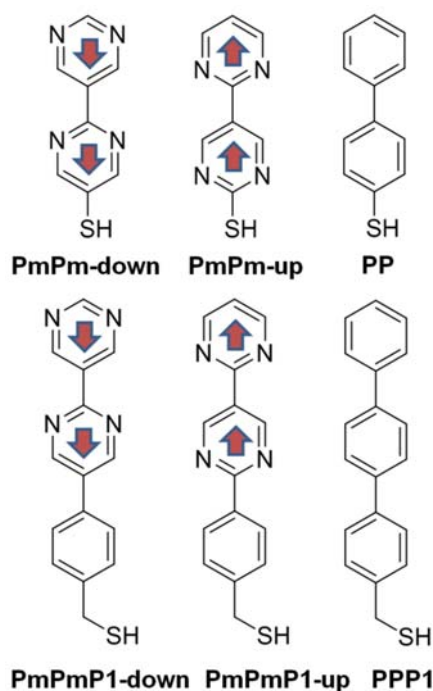


Figure 1. SAM-forming molecules used in this project along with their acronyms (**P** = phenyl, **Pm** = pyrimidine, **up/down** = direction of dipole moment (red arrows) with respect to the anchoring group). Note that PP and PPP1 were abbreviated differently in some of our earlier work (BPT/BP0 and TP1, respectively) but the new names are more consistent with the other acronyms used in the present study. The calculated components of the dipole moments of the isolated, gas-phase optimized molecules along the long molecular axis are -4.6 D for PmPm-down, $+4.3$ D for PmPm-up, $+0.6$ D for PP, -5.9 D for PmPmP1-down, $+3.2$ D for PmPmP1-up, and 0.0 D for PPP1. Notably, these dipoles don't simply change sign when inverting the orientation of the pyrimidine rings, especially in PmPmP1-up/down (where the contribution of the thiol dipole along the long molecular axis is very small). This is a consequence of the nitrogen atoms in the pyrimidines polarizing all surrounding atoms such that the asymmetry of their chemical environment (i.e., the relative location of the additional phenylene unit and the thiol) distinctly affects the net dipole moment (for more details see the Supporting Information).

The properties of the PmPm-up/down and PmPmP1-up/down SAMs were studied by a variety of complementary experimental techniques, including ellipsometry, contact angle goniometry, scanning-tunneling microscopy (STM), X-ray photoelectron spectroscopy (XPS), infrared reflection-absorption spectroscopy (IRRAS), near edge X-ray absorption fine structure (NEXAFS) spectroscopy, and Kelvin probe (KP). The experiments were accompanied by dispersion corrected density-functional theory (DFT) simulations, providing insight into the electronic structure within the SAMs at an atomistic level. The obtained results are compared to those for monolayers consisting of molecules with a single embedded pyrimidine group, viz. PPmP1-up/Au and PPmP1-down/Au¹³ as well as PmP-up/Au and PPm-down/Au^{15,18} (see Figure S1 in the Supporting Information).

2. Experimental Section

Chemicals and Synthesis Procedures. Solvents and chemicals necessary for the synthesis of the SAM precursors (Figure 1) were purchased from different vendors (see the Supporting Information) and used as received. PP and PPP1 were synthesized according to literature procedures.^{24,25} A short description of the synthesis procedures for PmPm-up/down and PmPmP1-up/down can be found in section 3.2. A detailed description of these procedures and the characterization data for the intermediates and final products are provided in the Supporting Information.

Precursors for the reference SAMs, viz. hexadecanethiol (HDT) and perdeuterated dodecanethiol (PDDT) were either purchased from Sigma-Aldrich (HDT) or synthesized from the respective bromoalkane using standard procedures (PDDT).

SAM Preparation. For most of the experiments, the SAMs were prepared on gold substrates purchased from Georg Albert PVD-Beschichtungen (Silz, Germany). These substrates were prepared by thermal evaporation of 30 nm of gold (99.99% purity) onto polished single-crystal silicon (100) wafers (Silicon Sense) that had been precoated with a 9 nm titanium adhesion layer. The films were polycrystalline, with predominant (111) orientation of individual crystallites and a RMS roughness value of 0.8 nm ($5 \times 5 \mu\text{m}^2$ scan area); in our experience, this value does not change noticeably upon SAM formation.

The SAMs used for all experiments except STM (see next paragraph) were formed by immersion of the substrates into solutions of the SAM precursors in either tetrahydrofuran (THF; Sigma-Aldrich) or ethanol (Sigma-Aldrich) for 24 h under nitrogen and at room temperature. After immersion, the samples were carefully rinsed with pure solvent and dried

under a flow of N₂. The SAMs prepared from both solvents did not show any significant differences; therefore, mostly the data for the growth from THF are shown. The reference HDT and PDDT SAMs were prepared on the same Au(111) substrates according to literature procedures.⁸

Substrates for the STM measurements were prepared differently, viz. by electron beam evaporation of gold onto mica substrates kept at 390 °C in ultra-high vacuum (UHV). The mica substrates were annealed for 4 hours at this temperature prior to deposition of gold and kept at this temperature for one hour afterwards. Then, the substrates were stored under nitrogen and annealed by pulling through a butane/air flame (1 Hz, 1 min) prior to the SAM preparation, promoting formation of large monoatomic terraces. To promote the formation of sufficiently large crystalline domains, elevated temperatures were applied either during or after SAM preparation. The best results regarding the STM analysis were achieved as follows: The PmPmP1-up samples were prepared by immersion of the substrates into a 0.1 mM solution of the respective precursor in pure ethanol for 1 hour at room temperature followed by annealing of the rinsed and blown dry substrate under nitrogen atmosphere at 60 °C for 10 h. The PmPmP1-down samples were prepared by immersion of the substrates into a 0.1 mM solution of the respective precursor in pure ethanol at 70 °C for 1 h.

Characterization - General Comments: The experiments were performed at room temperature. XPS and NEXAFS spectroscopy measurements were carried out under UHV conditions, with special care taken to minimize potential modifications of the SAMs induced by the primary X-rays.^{26,27}

Ellipsometry. A Sentech SE 400 ellipsometer equipped with a He/Ne laser (wavelength 632.8 nm, beam diameter 1-2 mm) was used to measure the effective thickness of the SAMs. The angle of incidence was 70° with respect to the sample surface normal. The complex refractive indices of the substrates, necessary for the data evaluation, were measured separately after a hydrogen plasma treatment for 2 min. The extinction coefficients of the monolayers were assumed to be zero, while the real part of the refractive index was set to 1.55, a value that, according to our experience, is well applicable in the case of mainly aromatic molecules.

STM. The measurements were conducted with a Bruker MultiMode8 SPM Nanoscope with Low-Current STM Converter (MMSTMLCE) and MultiMode V SPM Station under ambient conditions. The scanner had 1.4 × 1.4 μm² range. Tips were cut from a 0.25 mm thick Pt/Ir (4/1) wire. Molecular resolution images were scanned from different directions to eliminate thermal drifting and corrected by calibration with highly oriented pyrolytic graphite (HOPG).

IR spectroscopy. A Thermo Nicolet 6700 Fourier transform infra-red (IR) spectrometer with a narrow-band mercury cadmium telluride semiconductor detector was used to obtain all IR spectra. The resolution was 4 cm^{-1} and a constant flow of dry/ CO_2 -free air was applied through the optical path of the spectrometer. IRRA spectra of the monolayers were measured with p-polarized radiation at an angle of incidence of 80° relative to the sample surface normal. As reference, a PDDT SAM on Au was used. The IR spectra of the neat substances were acquired with a single-reflection diamond attenuated total reflection (ATR) unit.

IR spectra of the isolated molecules were calculated using DFT (Gaussian 09 program package²⁸ with the BP86 functional^{29,30} and the SVP basis set³¹), to support the assignment of the vibrational modes and to identify the directions of their transition dipole moments (TDMs). The calculated frequencies were not scaled.

XPS. The measurements were performed at the HE SGM beamline (bending magnet) of the synchrotron storage ring BESSY II in Berlin, Germany, using a custom-made experimental station.³² The spectra were acquired with a Scienta R3000 electron energy analyzer, in normal emission geometry. Primary X-ray energies of 350 eV and 580 eV were used; the energy resolution of the spectra was $\sim 0.3\text{ eV}$ and $\sim 0.6\text{ eV}$, respectively.

The binding energy (BE) scale of the spectra was referenced to the Au $4f_{7/2}$ emission at 84.0 eV.³³ Some of the spectra were fitted by symmetric Voigt functions and either a linear or a Shirley-type background. To fit the S $2p_{3/2,1/2}$ doublets, we used two peaks with the same full width at half-maximum (fwhm), a standard³³ spin-orbit splitting of $\sim 1.2\text{ eV}$ (verified by a fit), and a branching ratio of 2 (S $2p_{3/2}/S\ 2p_{1/2}$).

The intensities derived by the fitting were used to evaluate the effective thickness and packing densities of the monolayers. The procedure and all relevant parameters are described in detail in our previous publications.^{13,15} HDT/Au, having a well-defined thickness (1.92 nm) and packing density ($4.63 \times 10^{14}\text{ molecules/cm}^2$)³⁴, was used as reference.

NEXAFS Spectroscopy. The NEXAFS spectra were measured at the same beamline as the XP data. They were collected at the carbon and nitrogen K-edges in the partial electron yield (PEY) mode with retarding voltages of -150 V and -300 V , respectively. Linearly polarized synchrotron light with a polarization factor of $\sim 89\%$ was used as the primary X-ray source. The incidence angle of the X-rays was varied between normal (90°) and grazing (20°) incidence geometry to monitor the linear dichroism reflecting the molecular orientation in the SAMs.³⁵ The energy resolution was $\sim 0.3\text{ eV}$ at the C K-edge and $\sim 0.45\text{ eV}$ at the N K-edge. The photon energy (PE) scale was referenced to the pronounced π^* resonance of HOPG at 285.38 eV.³⁶

The spectra were corrected for the PE dependence of the incident photon flux and reduced to the standard form with zero intensity in the pre-edge region and a unity jump in the far post-edge region.

KP Measurements. Work function measurements were carried out using a UHV Kelvin Probe 2001 system (KP technology Ltd., UK). The measurements were performed under UHV conditions. As reference, we used a HDT/Au sample with the work function value set to 4.3 eV according to literature.¹⁴ The latter value was additionally verified by referencing it to the work function of freshly sputtered gold set to 5.2 eV.¹¹

Quantum Mechanical Simulations. The interfaces were modeled employing the FHI-aims code³⁷ using the PBE³⁸ functional combined with the surface version³⁹ of the Tkatchenko-Scheffler dispersion corrections scheme.⁴⁰ The systems were modeled using periodic boundary conditions and the repeated slab approach.⁴¹ The metal substrate was described using five layers of Au, of which the three bottom ones were held fixed in the geometry optimizations to avoid spurious relaxations. The dispersion corrections between the metal atoms were turned off. Two molecules were placed in a $(\sqrt{3} \times 3)$ rect unit cell in a herringbone fashion. For PmPmP1-down, also a cofacial arrangement of the molecules was tested. The dimensions of the unit cell in the x and y directions were defined according to the calculated Au lattice constant (4.158 Å, corresponding to a nearest neighbor distance of 2.940 Å) and held fixed in all the calculations. The dimension in the third spatial direction was defined such that a vacuum region of at least 20 Å was inserted between two consecutive slabs. The geometries were optimized employing a $9 \times 5 \times 1$ Γ -centered k-points grid. The C and N atoms were described using a “Tier 2” basis consisting of the minimal basis plus one set of basis functions up to d-functions and one set of basis functions up to g-functions. The H atoms were described using a “Tier 2” basis consisting of a minimal basis plus one set of basis functions up to p-functions and one set of basis functions up to d-functions. The S atoms were described using the minimal basis plus the full “Tier 1”, consisting of one set of basis functions up to f-functions, and the d- and g-functions of the “Tier 2” set of basis functions. The Au atoms were described using a “Tier 1” basis, consisting of the minimal basis plus one set of basis functions up to h-functions. The cutoff potential of all basis functions was set to 4 Å. Further details of the employed basis set can be found in the Supporting Information. The total energy criterion for the self-consistency cycle was set to 10^{-6} eV and the geometry optimizations were stopped when the maximum residual force component per atom was below 0.01 eV/Å.

The C 1s XP spectra were simulated within the initial state approach to avoid artifacts arising from combining periodic boundary conditions and the final state approach with explicit excitations in every unit cell.⁴² The latter would generate artificial dipolar layers, which would distort the spectra of the SAMs and render a comparison to experiments impossible. The spectra were modeled according to the procedure described in ref 42. The screening of the core-hole due the highly polarizable metal substrate was taken into account using an image potential model and assuming a dielectric constant of the SAMs of 3.9.⁴³ The contribution of every atom was weighted to account for the finite escape depth of the photoelectrons, using a damping factor β of 0.47. The individual contributions were artificially broadened using Gaussian functions with a variance of 0.15 eV.

Additional information regarding the initial geometries, the numerical settings, and the simulation of the XP spectra can be found in the Supporting Information.

The molecular dipoles were calculated for gas phase molecules using the code Gaussian 09, Rev D.01²⁸, employing the PBE functional²⁹ and the 6-311++g(d,p) basis set.

3. Results and Discussion

3.1. General Comments

Whereas consistent and well-reproducible experimental data were obtained for the PmPmP1-up/down SAMs, the data for the PmPm-up/down monolayers (and here especially for PmPm-up) exhibited significant scatter between multiple experimental series. Consequently, we consider the presented results for the latter films to be of only limited reliability. Therefore, we concentrate on the PmPmP1-up/down data in the presentation and analysis. For the PmPm-up/down monolayers only selected spectra and the most important extracted parameters are presented in the main manuscript. Additional data for these films can be found in the Supporting Information. Due to the *a priori* expected particularly high potential of these SAMs for devices (see section 1) we consider it useful to also present and shortly discuss these films in the present discussion.

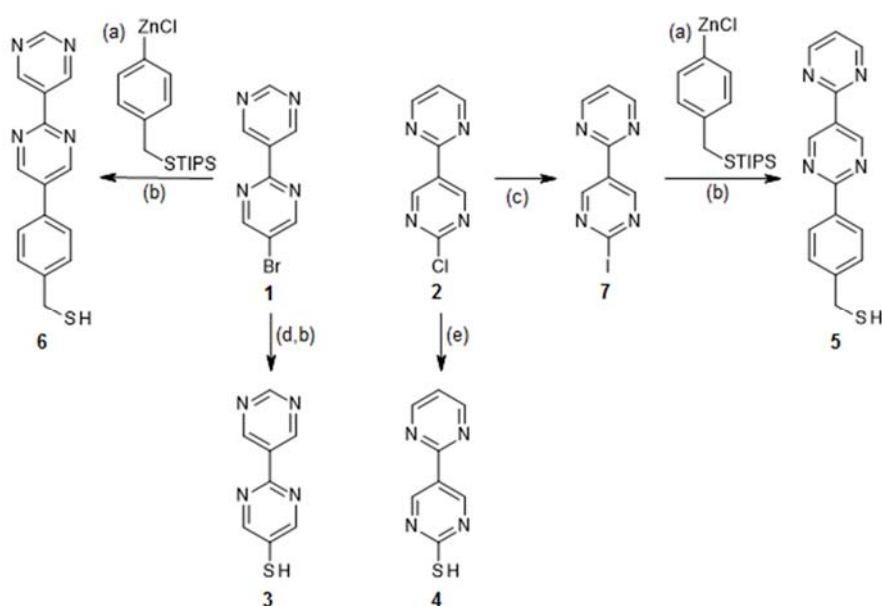
3.2. Synthesis

The major steps of the synthesis procedures are illustrated in Scheme 1. For the synthesis of the PmPm-up/down and PmPmP1-up/down molecules, two bipyrimidine building blocks had to be synthesized bearing a functional group either in 5 or 2'-position. As such moieties, 5-bromo-2,5'-bipyrimidine **1** and 2'-chloro-2,5'-bipyrimidine **2** were chosen. **1** was easily prepared by

Suzuki coupling of 5-bromo-2-iodopyrimidine with pyrimidine-5-boronic acid, while the synthesis of **2** was more complex. The Suzuki coupling of 2-iodopyrimidine with 2-chloropyrimidine-5-boronic acid gave low yields, presumably due to homocoupling reactions. Thereupon, the 2-isopropoxy-pyrimidine-5-boronic acid was synthesized enabling a Suzuki coupling in better yields to give 2-isopropoxy-2,5'-bipyrimidine, which can afterwards be converted to the desired product **2** by reaction with phosphoryl chloride.

2,5'-Bipyrimidine-5-thiol **3** was prepared by Pd-catalyzed cross coupling reaction of **1** with triisopropylsilylthiol (TIPSSH). The TIPS group was cleaved by reaction with HCl in MeOH to give the desired product **3**.

2,5'-Bipyrimidine-2'-thiol **4** was synthesized analogous to the preparation of pyrimidine-2-thiol described in literature.⁴⁴ Accordingly, educt **2** was reacted with sodium thiosulfate under acidic conditions. In contrast to **3**, which is a colorless solid, a yellow solid was obtained, indicating the formation of the corresponding thione.



Scheme 1. (a) PEPPSI IPr, THF; (b) HCl, MeOH; (c) HI, H₂O; (d) TIPSSH, LiHMDS, Pd(dppf)Cl₂, PhMe; (e) KH₂PO₄, H₃PO₄, Na₂S₂O₃, H₂O/EtOH. The precursors, intermediates, and target molecules are marked by numbers (see text for details).

The products 2'-(4-(mercaptomethyl)phenyl)-2,5'-bipyrimidine **5** and 5-(4-(mercaptomethyl)phenyl)-2,5'-bipyrimidine **6** were obtained from the corresponding TIPS-protected precursors. The latter were synthesized by a Negishi cross-coupling reaction from the corresponding bipyrimidine building blocks and the zinc organyl prepared from

4-bromobenzyl(triisopropylsilyl)sulfide.⁴⁵ While 5-bromo-2,5'-bipyrimidine **1** could be used directly, the 2'-chloro-2,5'-bipyrimidine **2** had to be converted to 2'-iodo-2,5'-bipyrimidine **7** to enable the cross-coupling reaction.

3.3. Crystallographic Data

Crystallographic data could be obtained for 5-bromo-2,5'-bipyrimidine **1**, 2'-chloro-2,5'-bipyrimidine **2**, PmPm-down **3**, and the corresponding disulfide of PmPm-up **4** (see Supporting Information). The most pronounced common features of the observed structures are (i) a coplanar or close-to-coplanar arrangement of the aromatic rings within individual molecules and (ii) an antiparallel arrangement of the adjacent molecules triggered by dipole-dipole interactions. On the basis of these data, a coplanar or close-to-coplanar molecular conformation can also be expected in the SAMs, especially, when they are densely packed. As to the antiparallel molecular arrangement, it should be hardly possible in the SAMs, since the molecules are forced to arrange in parallel because of their anchoring to the substrate through the docking group.

3.4. Ellipsometry

The ellipsometric thicknesses of the PmPm-down, PmPm-up, PmPmP1-down, and PmPmP1-up SAMs were determined as 1.1 ± 0.2 nm, 0.59 ± 0.04 nm, 1.38 ± 0.03 nm, and 1.49 ± 0.05 nm, respectively. These values are compiled in Table 1. They can be compared to the effective lengths of the molecules determined as the sum of the calculated length of the molecule and the length of the S–Au bond (estimated as ~ 0.24 nm)^{46,47}. The respective values are 1.23 nm for the PmPm-down and PmPm-up SAMs and 1.71 nm for the PmPmP1-down and PmPmP1-up monolayers.

Notably, the ellipsometric thickness values for the PmPm-down, PmPmP1-down, and PmPmP1-up SAMs are close to the effective lengths of the molecules, suggesting dense molecular packing and only a small inclination of the molecules in the SAMs. Conversely, the value for the PmPm-up monolayer is rather low, implying a limited monolayer quality and a loose molecular packing (see section 3.1).

Table 1. Effective thickness and packing density of the PmPm-up/down and PmPmP1-up/down SAMs, calculated on the basis of the ellipsometry and XPS data. The error of the packing density is estimated as $\pm 5\%$.

Monolayer	Effective thickness, nm (ellipsometry)	Effective thickness, nm (XPS)	Packing density, molecules/cm ²
PmPm-up	0.6 ± 0.1	0.8-1.0	2.6-3.5×10 ¹⁴
PmPm-down	1.1 ± 0.2	1.1 ± 0.2	4.4×10 ¹⁴
PmPmP1-up	1.5 ± 0.1	1.8 ± 0.2	4.6×10 ¹⁴
PmPmP1-down	1.4 ± 0.1	1.8 ± 0.2	4.7×10 ¹⁴

3.5. STM

The STM data for the PmPmP1-up/down SAMs are presented in Figure 2. The large scale images in Figures 2A and 2B show the formation of etch pits with diameters of 3-8 nm for both monolayers. The density of the etch pits is higher for PmPmP1-down/Au, but they are on the average smaller than those for PmPmP1-up/Au. A typical diameter of the domains with ordered molecules is ~5 nm, with the domains in PmPmP1-down/Au being generally smaller and harder to image than for PmPmP1-up/Au. Note that omitting the additional annealing step (PmPmP1-up/Au; see section 2) or preparation at room temperature (PmPmP1-down/Au; see section 2) resulted in larger, but more disordered domains for both SAMs which made it hardly possible to achieve molecular resolution. Note that a comparison of the STM micrographs of the SAMs prepared at room temperature with those of the SAMs treated at higher temperatures yields no significant structural differences (see Figure S24 in the Supporting Information).

Figures 2a and 2b show ordered domains of PmPmP1-up/Au and PmPmP1-down/Au with molecular resolution. For PmPmP1-up/Au (Figure 2a), the height profiles indicate 0.50 nm (line scan 1) and 0.60 nm (line scan 2) distances between the molecules appearing with equal heights. The elongated distances in the profile (line scan 2) are most likely related to thermal drift. This basic structural motif corresponds to the $(\sqrt{3} \times \sqrt{3})R30^\circ$ arrangement with a packing density of 4.6×10^{14} molecules/cm² (Figure 2c, left), as commonly observed for oligophenylene-thiolate derived SAMs.⁴⁸⁻⁵³ A similar packing density was observed for PmPmP1-down/Au (Figure 2b). The detailed structure is difficult to identify, but the increased distance between equivalent molecules in the direction of the line scan 4 (1.1 nm) indicates a doubling of the unit cell (then containing two molecules as found also for the cases of PPP1 and PPP).⁵³⁻⁵⁵ In contrast to these cases, the tails of the molecules do not all lie on the cell vectors (Figure 2c, right) as observed already for PmPmP1-down/Au.¹³

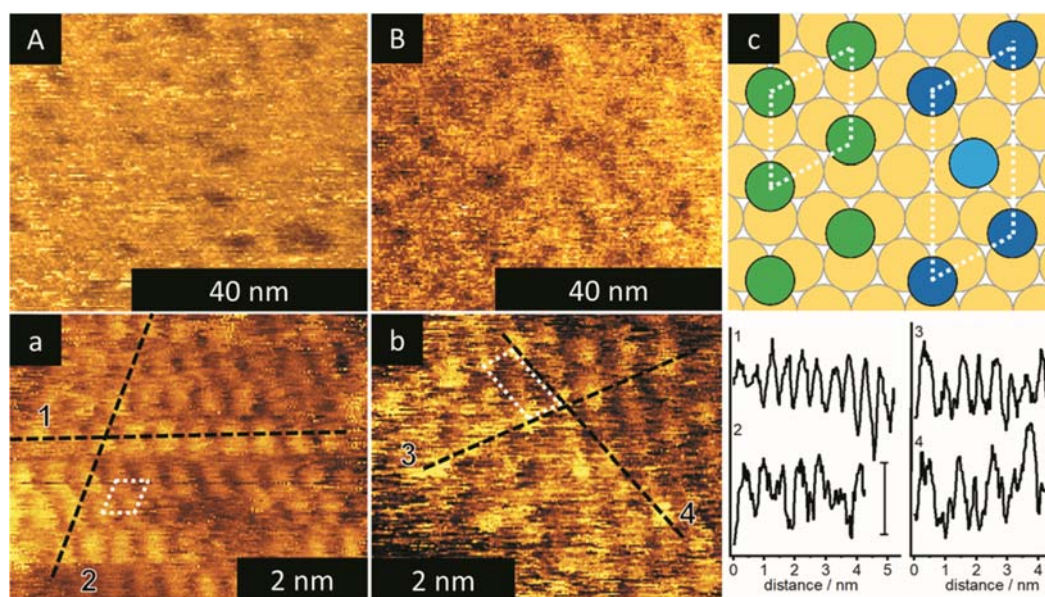


Figure 2. Large scale (A, B) and high magnification (a, b) STM images of PmPmP1-up (A, a) and PmPmP1-down (B, b) SAMs, together with cross-sectional height profiles (marked by numbers) along the dashed lines shown in a and b. The directions of the height profiles correspond to the $\langle 11-2 \rangle$ and equivalent directions of the Au(111) surface. The vertical scale bars in the height profiles correspond to an apparent height of 0.1 nm. Measurement conditions: 5 pA, 500 mV (A); 17 pA, 370 mV (a); 3 pA, 300 mV (B); 26 pA, 170 mV (b). The proposed positions of the tail groups of the molecules in the unit cells are shown in c using green (PmPmP1-up) and blue (PmPmP1-down) circles.

3.6. XPS

Representative Au 4f, S 2p, C 1s, and N 1s XP spectra of the PmPmP1-up/down and PPP1 SAMs are shown in Figure 3. Analogous spectra of the PmPm-up/down monolayers can be found in the Supporting Information (Figures S25 and S26).

The Au 4f spectra of all three SAMs in Figure 3a exhibit a similar intensity, which suggests that effective thicknesses and packing densities of the PmPmP1-up and PmPmP1-down monolayers are similar and close to those for the densely packed and well-oriented, reference PPP1 SAM (see e.g. refs 13 and 23).

The S 2p spectra of all three SAMs in Figure 3b exhibit a single S 2p_{3/2,1/2} doublet at ~ 162.0 eV (S 2p_{3/2}). This BE is characteristic of the thiolate species bound to noble metal substrates,³² indicative of the distinct SAM character of all the studied films. The intensity of the doublet is similar for all three SAMs, suggesting similar packing densities. As it will be discussed later, it is important to point out that no traces of unbound thiol groups can be found in the spectra.

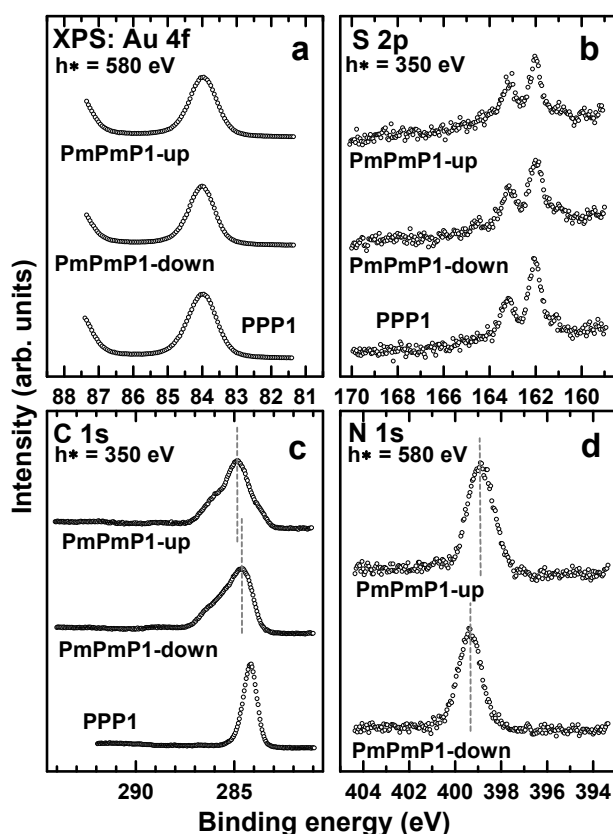


Figure 3. Au 4f (a), S 2p (b), C 1s (c), and N 1s (d) XP spectra of the PmPmP1-up/down and PPP1 (reference) SAMs. The spectra were acquired at photon energies of 350 eV (b, c) and 580 eV (a, d). The vertical dashed lines are guides to the eye. The low signal-to-noise character of the S 2p spectra is related to a strong attenuation of the photoelectron signal by the thick and densely packed SAMs.

The C 1s spectra of the PmPmP1-up/down SAMs in Figure 3c are quite complex compared to the spectrum of the reference PPP1 monolayer. They represent a superposition of the contributions from the phenyl and pyrimidine rings with the positions of the peaks not only affected by the standard chemical shifts but also by electrostatic effects, typical of the pyrimidine-substituted SAMs.^{13,15,18}

These effects will be discussed in detail below (section 3.11) using theoretical calculations. The contribution of the phenyl ring is strongly suppressed by the attenuation effects.⁵⁶ It represents a single peak at 284.15-284.2^{26,57} as seen for the example of PPP1/Au. The contribution of the pyrimidine rings, which dominate the spectra, can be rationalized on the basis of literature gas phase data.⁵⁸ Accordingly, it should represent a superposition of three peaks with an intensity ratio of 1:2:1 and BEs differing by 1.0 eV and 1.4 eV, respectively. The position of the low BE

peak should be located close to the phenyl-stemming feature, assuming the same BE shift upon transition from the gas phase to the solid state as for CO₂ taken in ref 58 as reference (the solid state data for CO₂ can be found in ref 59).

The spectrum of PmPmP1-down/Au indeed represents such a “1:2:1” shape, with a dominant peak in the middle and the less intense "shoulders" at the low and high BE sides. The spectrum of PmPmP1-up/Au exhibits a shift of the main peak to lower BE, which is most likely related to electrostatic effects caused by the dipolar pyrimidine moiety. Indeed, as shown in our previous work,^{13,15} pyrimidine moieties with upward oriented dipoles shift the C 1s peaks for carbon atoms located above the dipoles to higher BEs, while the opposite is the case for downward oriented dipoles. This is consistent with the observations in Figure 3c, even though the extent of the shift, ~0.3 eV, is noticeably smaller than in the case of embedded individual pyrimidine groups, viz. ~1.1 eV for PPmP1-up/Au and PPmP1-down/Au.¹³ This suggests a lesser extent of the electrostatic effects for the SAMs of the present study, as will be discussed in detail in section 3.11.

The N 1s spectra of the PmPmP1-up/down SAMs in Figure 3d exhibit a single peak, associated with the nitrogen atoms in the pyrimidine moieties. The fwhm of this peak is ~1.4 eV for PmPmP1-up/Au and ~1.2 eV for PmPmP1-down/Au, which is noticeable larger than the respective parameter for SAMs consisting of molecules with a single embedded pyrimidine group (~0.9 eV)²⁷. This means that the contributions of the successive pyrimidine rings appear at slightly different BEs, merging in the comparably broad joint peak and becoming indistinguishable. Significantly, the intensity of this peak is similar for the "up" and "down" monolayers suggesting similar packing densities. The BE position of this peak for PmPmP1-up/Au, 398.9-399.0 eV, is somewhat different from that for PmPmP1-down/Au, 399.2-399.3 eV. Interestingly, the BE shift with respect to the dipole orientation is opposite to that observed in the C 1s spectra. This also means that, the shift of the N 1s peaks goes in the direction opposite to what would be expected based on the electrostatic shifts due to the molecular dipole moments.⁴² Possible reasons for this behavior will be discussed in section 3.12.

The O 1s spectra of the PmPmP1-up/-down and PPP1 (reference) SAMs are shown in the Supporting Information (Figure S27). The spectrum of the reference PPP1/Au shows nearly zero signal, while the spectra of the PmPmP1-up SAMs exhibit a weak but distinct O 1s signal. The signal is noticeably stronger in the case of PmPmP1-down and has its major spectral weight at ~533 eV. That signal can be tentatively ascribed to H-bridge bound H₂O.⁶⁰

In addition to the qualitative discussion of the spectra, they were also quantitatively analyzed to determine the effective thickness and packing density of the SAMs (see section 2 for details). The obtained values are compiled in Table 1. The effective thickness values for the PmPmP1-up/down SAMs are similar to the molecular lengths (see section 3.2), suggesting dense molecular packing and nearly upright molecular orientation. Similar values were observed for the analogous SAMs consisting of molecules with a single embedded pyrimidine group, viz. PPmP1-up/Au and PPmP1-down/Au.¹³

The effective thickness value for PmPm-down/Au is also close to the molecular length, while for PmPm-up/Au the measured values for the effective thickness exhibited significant scattering in different experimental series and should, therefore, be taken with caution.

As for the packing density, the XPS-derived values for the PmPmP1-down/Au and PmPmP1-up/Au are quite similar and very close to the value of 4.6×10^{14} molecules/cm² obtained by the STM measurements (section 3.5). Note that similar packing densities are commonly observed for oligophenyl SAMs, see e.g. refs 48-53, including those with embedded pyrimidine moieties (see e.g. ref 13). The packing density of PmPm-down/Au is somewhat lower but still corresponds to dense molecular packing. The packing density of PmPm-up/Au is noticeably lower, again suggesting a limited quality of this particular SAM.

3.7. Contact Angle Measurements

Advancing (red circles) and receding (blue squares) water contact angles (WCAs) for the PmPm-up/down and PmPmP1-up/down SAMs are presented in Figure 4. The WCA values for the PmPmP1-up SAM correlate well with the analogous values for the previously discussed PmP-up monolayer,¹⁵ in which the terminal pyrimidine ring has the same orientation. At the same time, the WCA values for the PmPm-up SAM are distinctly different, with a much larger hysteresis. This is one more indication for a lower quality of this particular film films.

The WCA values for the "down" SAMs are smaller by 20-40° than those for the "up" monolayers, which correlates with the expected SAM structure, viz. a location of the nitrogen atoms closer to the SAM-ambient interface in the case of "down" monolayers. In addition, the WCA values for the PmPm-down and PmPmP1-down SAMs are quite similar, suggesting a similar quality and molecular packing of these films.

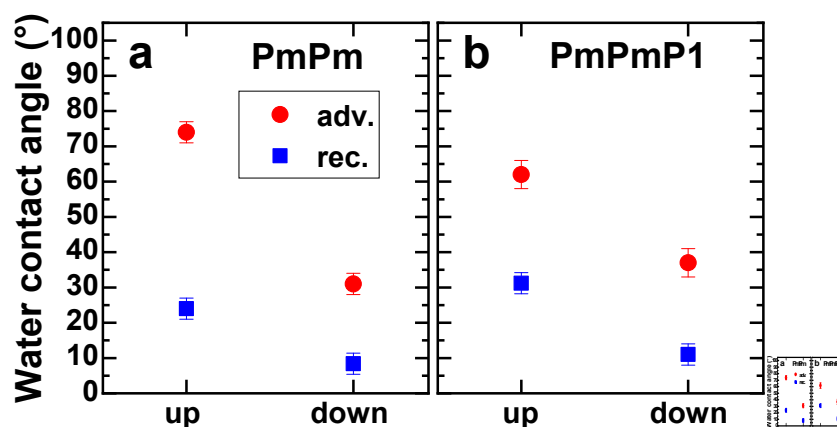


Figure 4. Advancing (red circles) and receding (blue squares) water contact angles for the PmPm-up/down (a) and PmPmP1-up/down (b) SAMs.

3.8. IRRAS

In Figure 5, the IR spectra of the PmPm-up/down and PmPmP1-up/down systems are compiled. For each molecule, the IRRA spectrum is compared to the ATR-IR spectrum of the bulk material and a calculated IR spectrum of the isolated molecule. Because of the tautomerism of PmPm-up,^{61,62} two calculated spectra are depicted, one of the thiol isomer, the other one of the thione isomer.

Aided by the DFT calculations, the most important absorption bands in the IR spectra are assigned to the corresponding vibrational modes along with the directions of the transition dipole moments (TDMs) relative to the molecular plane and the long molecular axis (see Tables S1-S4 in the Supporting Information).

PmPmP1-up/down. When comparing the ATR data to the IRRA spectra in Figures 5a and 5b, it becomes evident that the relative signal strengths of the vibrational bands mainly vary in a systematic manner. According to the surface selection rule on metals,⁶³ one can expect a (partial) extinction of the IRRA signal for vibrational modes, whose TDMs are oriented (mostly) parallel to the surface. Therefore, for molecules standing (nearly) upright, vibrations with TDMs parallel to the long molecular axis (labeled “||”) are unaffected while all bands with a TDM perpendicular to the long molecular axis (labeled “⊥” for perpendicular in-plane and “oop” for perpendicular out-of-plane) are attenuated. This is indeed the case in the spectra of the PmPmP1-down and PmPmP1-up systems in Figures 5a and 5b, respectively. The almost complete attenuation of the oop bands 8a, 9a and 7b for the SAMs as compared to the neat substances is most striking. This suggests a nearly upright molecular orientation in the SAMs, in agreement with all other experimental data. Note that in principle it is possible to go beyond

this qualitative statement and obtain the tilt angle of the molecules in the SAMs by the analysis of the relative intensities of bands with TDMs of three independent directions (\parallel , \perp and oop) using a method established by Parikh and Allara.⁶⁴ However, for the systems studied here, such an evaluation is rendered impossible by several reasons, like the impossibility to identify isolated \perp bands and also by band position shifts that lead to the merge of vibrational mode signals in the IRRA spectra (e.g., in the case of the ν CN, δ CH band at 1386 cm^{-1} in the spectrum of the PmPmP1-up neat substance that we believe to coincide with the 1415 cm^{-1} band in the IRRA spectrum of this species).

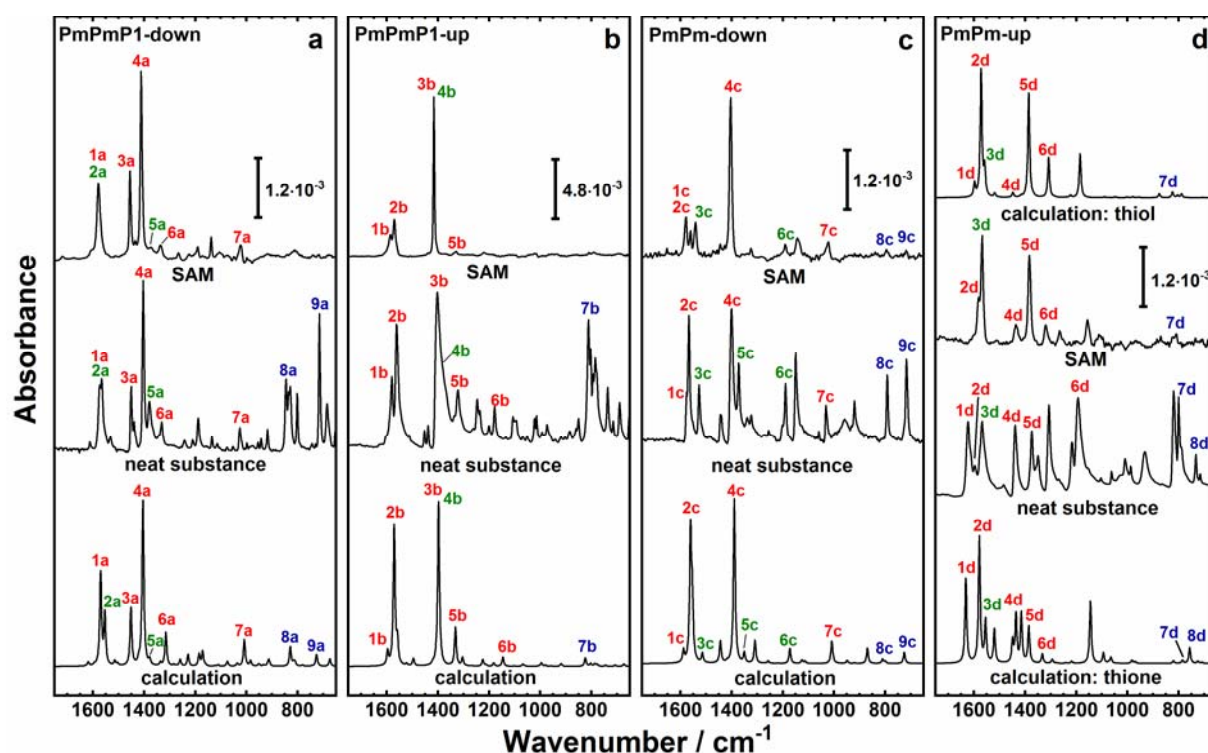


Figure 5. IRRA (SAM), ATR-IR (neat substance) and DFT calculated spectra of the PmPmP1-down (a), PmPmP1-up (b), PmPm-down (c) and PmPm-up (d) systems. Absorbance scale bars are given for the IRRA spectra. The calculated spectra are displayed in arbitrary units. Most prominent and important vibrational modes are labeled (see text and Tables S1-S4 in the Supporting Information for the assignments). The labels are color-coded in accordance with the TDM orientation (see text for details): \parallel - red, \perp - green, and oop - blue.

PmPm-down. Similar to the PmPmP1-up/down case, the spectra of PmPm-down in Figure 5c exhibit attenuation of oop bands, like 8c and 9c, and some \perp bands, like 6c, when comparing the neat substance and the SAM. This again suggests a nearly upright molecular orientation in the SAMs. Note, however, that some \parallel bands, like 2c, seem to be attenuated as well, giving rise

to certain inconsistencies. This might be caused by an ambiguity in the assignment of the bands in the given region of the spectrum.

PmPm-up. As mentioned above, in Figure 5d, besides the calculated spectrum for the thiol form of PmPm-up, also the one for the thione form is depicted, in view of the thiol-thione tautomerism of this species.^{61,62} It is expected that the calculated thiol spectrum is more similar to the IRRA spectrum of the SAM, where no thione tautomer can form due to the release of the proton and formation of the gold-thiolate bond. Conversely, the ATR spectrum should be more comparable to the calculated thione spectrum, since the thione seems to be the dominant species in the solid state. These expectations are indeed met by the spectra, as is evident from Figure 5d and Table S4. In particular, a prominent symmetric C–N stretching mode (band 1d), characteristic of a thione moiety, cannot be found in the spectrum of the SAM. The same is true for the N–H wagging mode (band 8d), which is present in the calculated spectrum of the thione and in the ATR spectrum of the neat substance, but is absent in the spectrum of the SAM.

Notably, in the spectrum of the PmPm-up SAM, the asymmetric C–N-stretching band 3d (TDM: \perp) is not attenuated compared to other modes with TDMs parallel to the long molecular axis, whereas the oop-modes like 7d and 8d are strongly attenuated. This suggests that the molecules, being generally oriented upright, are, on average, inclined relative to the surface normal within the molecular plane.

3.9. NEXAFS Spectroscopy

C and N K-edge NEXAFS data for the PmPmP1-up/down and PPP1 (C K-edge only) SAMs are presented in Figures 6 and 7, respectively. The analogous data for the PmPm-up/down SAMs can be found in the Supporting Information (Figures S28 and S29). There are two kinds of data, viz. the spectra acquired at an X-ray incidence angle of 55° (magic angle) and the curves corresponding to the difference between the spectra collected under normal (90°) and grazing (20°) incidence. These data provide complementary information: While the 55° spectra are exclusively representative of the electronic structure of the films, the difference curves are characteristic of molecular orientation and orientational order in the monolayers.³⁵

The 55° C K-edge spectra of the PmPmP1-up/down SAMs in Figure 6 contain contributions from the pyrimidine and phenyl rings. The pyrimidine contribution dominates, because of the larger number of the pyrimidine groups and a stronger attenuation of the PEY signal from the deeper-lying phenyl ring. The latter contribution is well represented by the spectrum of PPP1/Au, with a clear dominance of the intense and sharp π_1^* resonance at ~285.0 eV (**1**) and

a variety of comparably weak π^* and Rydberg resonances as well as broader σ^* resonances at higher excitation energies (see refs 35 and 65-67 for the assignments). According to literature,^{68,69} the spectrum of pyrimidine is dominated by a complex π^* feature, with maxima at 284.7-285.1 eV (**2**; low intensity), 285.4 eV (**3**; high intensity), and 285.86 eV (**4**; intermediate intensity). The spectrum exhibits also a variety of comparably weak π^* and Rydberg resonances as well as broader σ^* resonances at higher excitation energies (see refs 68 and 69 for the assignments).

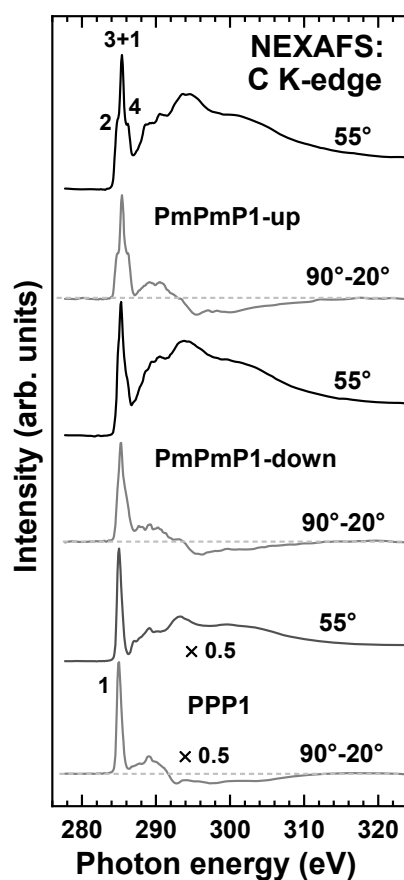


Figure 6. C K-edge NEXAFS spectra of the PmPmP1-up/down and PPP1 (reference) SAMs acquired at an X-ray incidence angle of 55° (black lines), along with the respective difference between the spectra collected under the normal (90°) and grazing (20°) incidence geometry (gray lines). Individual absorption resonances are marked by numbers (see text for the assignments). The horizontal dashed lines correspond to zero.

The above triple π^* -resonance features are indeed observed in the 55° C K-edge NEXAFS spectra of the PmPmP1-up/down SAMs in Figure 6, even though the relative weights of the individual contributions are somewhat different for the "up" and "down" case. This is related to either upwards or downwards orientation of the pyrimidine rings within the molecular

backbone, resulting in somewhat different attenuation of the PEY signals from the individual carbon atoms associated with the particular π^* -components within the overall π^* -feature.^{68,69}

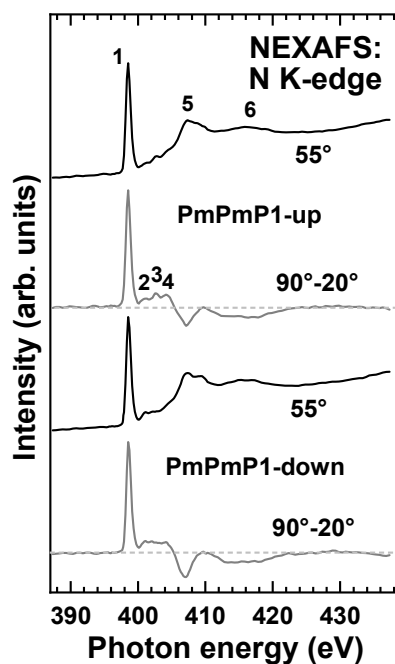


Figure 7. N K-edge NEXAFS spectra of the PmPmP1-up/down SAMs acquired at an X-ray incidence angle of 55° (black lines), along with the respective difference between the spectra collected under the normal (90°) and grazing (20°) incidence geometry (gray lines). Individual absorption resonances are marked by numbers (see text for the assignments). The horizontal dashed lines correspond to zero.

The 55° N K-edge spectra of the PmPmP1-up/down SAMs in Figure 7 are typical of pyrimidine.^{68,69} The spectra are dominated by a strong π^* resonance at ~398.5 eV (**1**) accompanied by several low intensity π^* and mixed π^* -Rydberg features at 401 eV (**2**), 402.6 eV (**3**) and 404.3 eV (**4**) as well as a variety of resonances at higher excitation energies (**5** and **6**). The intensities of the most prominent π^* resonance are similar for the "up" and "down" cases, supporting, in accordance with all other data, similar packing densities.

The difference spectra in Figures 6 and 7 exhibit pronounced peaks at the positions of the characteristic absorption resonances, which suggests a high orientational order in the PmPmP1-up/down SAMs. The signs of these peaks, which are positive for the π^* resonances and negative for the σ^* ones, imply a largely upright molecular orientation in the SAMs (in view of the fact that the TDMs of the $1s \rightarrow \pi^*$ and $1s \rightarrow \sigma^*$ excitations are directed perpendicular and parallel to the plane of the pyrimidine and phenyl rings, respectively).

Table 2. Average tilt angles of the π^* orbitals of the PmPm-up/down and PmPmP1-up/down SAMs, calculated on the basis of the C K-edge and N K-edge NEXAFS data. The accuracy of the values is estimated to be $\pm 3^\circ$.

Monolayer	Tilt angle (α) from the C K-edge data	Tilt angle (α) from the N K-edge data	Average value
PmPm-up	68°	71°	69.5°
PmPm-down	74°	78°	76°
PmPmP1-up	72°	75°	73.5°
PmPmP1-down	73°	78°	75.5°

The above qualitative considerations were complemented by a quantitative analysis of the NEXAFS data, monitoring the intensities of the most prominent π^* resonances in the spectra. The data were processed within the standard theoretical framework for vector-like orbitals, like π^* ones.³⁵ Accordingly, the intensity of a particular π^* resonance was plotted versus the X-ray incidence angle and fitted by a suitably chosen theoretical curve, looking for an optimal value of the average tilt angle of the π^* orbital with respect to the surface normal, α .^{57,67} The derived values of the average tilt angle, determined on the basis of the C and N K-edge data, are shown in Table 2, with the C K-edge and N K-edge derived values being representative of the orientation of the entire molecular backbone and its bipyrimidine part, respectively. The similarity of these values suggests a coplanar or close-to-coplanar molecular conformation in the SAMs, in agreement with the crystallographic data (see section 3.3) but also typical of densely packed aromatic monolayers⁵⁷ including pyrimidine-substituted SAMs.^{13,15}

Based on the average tilt angles of the π^* orbitals, average molecular tilt angles with respect to the surface normal, β , could be calculated using the following equation: $\cos \alpha = \sin \beta \times \cos \gamma$, where γ corresponds to the molecular twist angle describing the rotation of the molecular backbone around the molecular axis. It is zero, when the plane in which the molecules are tilted is perpendicular to the molecular plane.⁷⁰ This angle can be determined from NEXAFS data only in the presence of certain functional groups, which are not present in the molecules studied here.⁷⁰ It can, however, be estimated within reasonable assumptions on the basis of the bulk

structure, or determined from IRRAS¹³ or modelling data. In the present case, we will rely on the latter, as discussed in detail in section 3.11.

3.10. Work Function

The work function values for the PmPm-up/down and PmPmP1-up/down SAMs on Au(111) are presented in Figure 8. The pyrimidine groups have a clear effect on the work function, shifting it downwards and upwards with respect to PP/Au and PPP1/Au, in agreement with the direction of the dipole moment. The shift for PmPm-down/Au and PmPmP1-down/Au are rather similar. Conversely, the shift for PmPm-up/Au is noticeably smaller than that for PmPmP1-up/Au. This is fully consistent with the limited quality of the PmPm-up SAM.

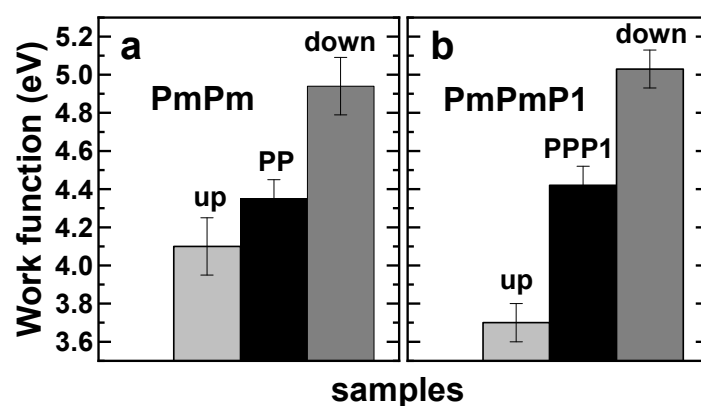


Figure 8. Work function values for the PmPm-up/down (a) and PmPmP1-up/down (b) SAMs deposited from ethanol.

The absolute value of the shift (relative to the PPP1 reference SAM) amounts to -0.72 eV for the PmPmP1-up and $+0.61$ eV for the PmPmP1-down monolayer. This means that depending on the dipole orientation, the work function can be changed over a sizable energy range of ~ 1.35 eV. For comparison, a single embedded pyrimidine group in the PmP-up and PmP-down monolayers gives work function shifts of -0.37 eV and $+0.52$ eV, respectively (~ 0.9 eV difference);¹⁵ while for the PmP1-up and PmP1-down SAMs the shifts are -0.42 eV and $+0.56$ eV, respectively (~ 1.0 eV difference).¹³ This means that by doubling the number of pyrimidine groups, the spread of the achievable work functions increases only by a factor of 1.35-1.4. This implies that the effect of the pyrimidine units on the accessible work function range does not scale linearly with their number. Notably, this sublinear increase of the work function is particularly pronounced for the down-orientation of the pyrimidine dipoles. I.e., while the work-function change (relative to the reference SAMs) nearly doubles in the up-case

when going from the monopyrimidine systems (PmP-up and PPmP1-up) to the bipyrimidine case (PmPmP1-up), the work-function changes for all down-systems (PmP-down, PPmP1-down, and PmPmP1-down) are nearly same, i.e., within 0.09 eV (in spite of the particularly large molecular dipole of PmPmP1-down, see caption of Figure 1). Possible reasons for this behavior will be discussed in section 3.12. Prior to that, the most important results of the quantum-mechanical simulations shall be shown.

3.11. Simulations

As in the experimental section, we will also here focus on the PmPmP1-up/down SAMs.

Modeling the structural properties of the SAMs.

The optimized geometries of the PmPmP1-up and PmPmP1-down SAMs are shown in Figure 9. As reported in the methodology section, the SAMs were modelled using a $(\sqrt{3} \times 3)$ rect unit cell, which is equivalent to a $(\sqrt{3} \times 2\sqrt{3})R30^\circ$ cell (as observed for PmPmP1-down), but computationally more easily accessible due to the orthogonal lattice vectors. This surface unit cell is also consistent with the $(\sqrt{3} \times \sqrt{3})R30^\circ$ packing motif observed in STM for PmPmP1-up, when considering unit cells containing two molecules, which in this system cannot be distinguished in the STM experiments. These molecules could adopt a herringbone or a cofacial arrangement, with the herringbone case being energetically more stable (by ~ 0.1 eV/molecule). The molecules in the SAM assume an almost perfectly planar conformation, with inter-ring torsions below 2° and 3° for PmPmP1-up and PmPmP1-down, respectively. This is again consistent with the conclusions drawn from the experiments (cf., crystallographic data reported in section 3.3).

The simulated optimized geometries of Figure 9 were used to obtain the tilt angles of the π^* orbitals α , the molecular tilt angles β and the molecular twist angles γ (see section 3.9 and ref 15 for a more thorough definition of α , β and γ). The values are reported in Table 3, where the subscripts 1 and 2 refer to the two inequivalent molecules in the simulation unit cell. For α also the average value α_{av} is given, calculated via $\cos^2\alpha_{av} = (\cos^2\alpha_1 + \cos^2\alpha_2)/2$ to be consistent with the evaluation of the experimental NEXAFS data.³⁵

The calculated average values of the tilt angles of the π^* orbitals are very similar for both systems and agree fully with the experimental data in Table 2. Also the values of the tilt angles, β , are very close, which is consistent with ellipsometry (section 3.4) and XPS (section 3.6) yielding a similar thickness of both SAMs. The simulated twist angles γ are very different for the two inequivalent molecules in the unit cell, which we associate with the herringbone

arrangement of the molecules (cf., Figure 9). The very different values of γ result in significantly different angles of the molecular π -planes for the two molecules in the unit cells in spite of the essentially identical tilts. These different orientations of the π -planes are tentatively associated with the observation in the STM pictures of PmPmP1-up that not all of the observed features lie on the unit-cell axis.

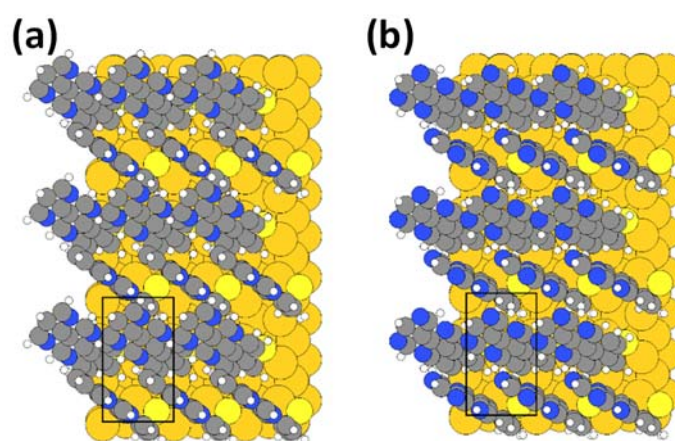


Figure 9. DFT optimized structures of the PmPmP1-up (a) and PmPmP1-down (b) SAMs. Color code: H – white, C – grey, N – blue, S – light yellow, Au – dark yellow.

Table 3. DFT calculated average tilt angles of the π^* orbitals α , molecular tilt angles β and molecular twist angles γ of the PmPmP1-up/down SAMs. The subscripts 1 and 2 refer to the two inequivalent molecules in the unit cell. α_{av} is obtained by averaging α_1 and α_2 as described in the main text.

Monolayer	$\alpha_{av} / ^\circ$	$\alpha_1 / ^\circ$	$\alpha_2 / ^\circ$	$\beta_1 / ^\circ$	$\beta_2 / ^\circ$	$\gamma_1 / ^\circ$	$\gamma_2 / ^\circ$
PmPmP1-up	74.30	87.27	67.73	24.80	23.17	83.34	15.59
PmPmP1-down	75.30	87.38	69.09	25.11	23.54	83.81	26.68

Simulated work function changes

To analyze the simulated electronic properties of the PmPmP1-up/down SAMs, in Figure 10 we compare the measured and calculated work function changes with respect to the reference non-polar PPP1 SAM. For the sake of comparison, also data for the related monopyrimidine monolayers, PPmP1-up/down, are shown.¹³ They differ from PmPmP1-up/down only in the terminal ring being a phenyl group.

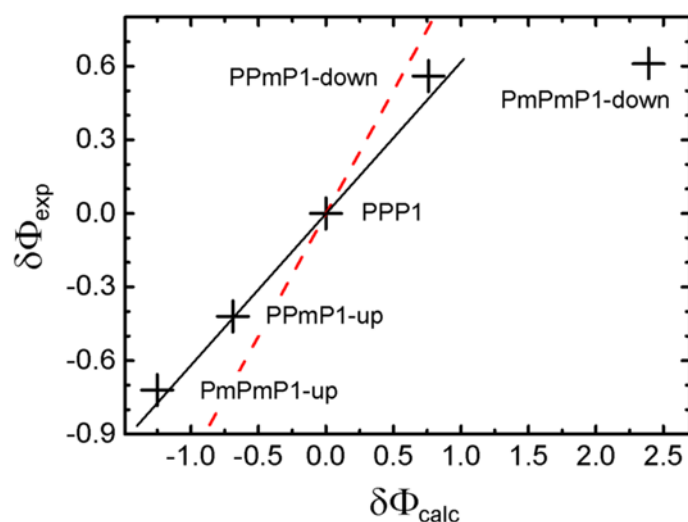


Figure 10. Comparison between the measured ($\delta\Phi_{\text{exp}}$) and calculated ($\delta\Phi_{\text{calc}}$) work function changes of PmPmP1-up/down and PPmP1-up/down SAMs on Au(111) relative to a PPP1 reference SAM (origin). As a guide to the eye, a dashed red line with a slope of 1 is plotted. The black line is a linear fit through the origin (PPP1) to the data for the PmPmP1-up and PPmP1-up/down SAMs.

The data in Figure 10 allow several conclusions: For PmPmP1-up, PPmP1-up, and PPmP1-down there is a close to linear relation between the measured and calculated work function changes. A linear fit through the corresponding data points (and the origin; black line) yields a slope somewhat smaller than one (dashed red line). This is in line with previous observations, where we have consistently observed a minor overestimation of the SAM-induced work function change in the simulations.^{13,15} This has in part been attributed to residual disorder at grain boundaries and to shortcomings of the employed computational methodology. As already indicated in section 3.10, PmPmP1-down does not follow that trend. In fact, in the simulations we find that replacing the terminal phenyl ring of PPmP1-down by a pyrimidine group with downwards-oriented dipole massively increases the calculated work function change such that $\delta\Phi_{\text{calc}}$ more than doubles from PPmP1-down to PmPmP1-down. This is consistent with the evolution of the molecular dipoles (see caption of Figure 1 and the Supporting Information). Conversely, in the experiments, the additional pyrimidine ring hardly impacts the value of $\delta\Phi_{\text{exp}}$. Possible reasons for that will be discussed below in section 3.12.

As far as the simulations per se are concerned, the question remains, why the calculated change in the work function even for the “ideal situation” does not scale linearly with the number of pyrimidine rings in the backbone (it increases by a factor of more than three between PPmP1-down and PmPmP1-down and only by a factor of 1.8 in the “up” case). This observation

can be rationalized by the fact that in our simulations the dipole moment of a pyrimidine ring significantly depends on its chemical surroundings, which is discussed in detail in the Supporting Information. This results in an evolution of the molecular dipoles that mimics that of the work function changes.

Simulated XP spectra

The simulated C 1s XP spectra of the PmPmP1-up, PmPmP1-down, and the reference PPP1 SAMs are shown in Figure 11a. These spectra were corrected for the damping according to a primary photon energy of 580 eV (see the Supporting Information) and shifted by 19.0 eV towards larger binding energies to make the simulated and the experimental spectra of the reference PPP1 SAM lie on top of each other. Such a shift has to be applied since the spectra are simulated using the initial state approach, that treats Kohn-Sham energies as orbital energies. Kohn-Sham energies are nonetheless known to well reproduce energetic shifts of inequivalent atoms (i.e., they need to be considered with respect to a reference system).⁷¹⁻⁷⁴ The magnitude of the shift of the spectra applied here is consistent with what is typically observed for SAMs.^{15,75} To interpret the spectra, it is again useful to consider the binding energies associated with the individual carbon atoms. These are shown in Figure 11b (where screening of the core hole by the metal and the above-described rigid shift have been considered).

The binding energies for the lowest rings in all three systems are essentially equal, which is not surprising considering that these rings are chemically identical and that also the collective electrostatic shifts of the binding energies caused by the thiolate dipoles are the same in all cases.⁴² For the other rings, the interpretation of the XP spectra is complicated by the fact that the electrostatic shifts⁴² induced by the 2D assemblies of pyrimidine-related dipoles between the substrate and the respective atoms cause different electrostatic shifts of the binding energies for the different SAMs. Moreover, there are chemical shifts especially increasing the binding energies of the carbon atoms bonded to nitrogen atoms. This is clearly resolved for the central rings of the PmPmP1-up/down SAMs with the effect being most pronounced for carbon atoms bonded to two nitrogen atoms.

The impact of shifts due to collective electrostatic effects becomes apparent for the topmost pyrimidine ring. Thus, for PmPmP1-up all features are shifted to even higher binding energies than in the central ring. Consistent with an overestimation of the work function change (see above) this electrostatic shift is larger in the simulations than in the experiments. As a consequence, the intensities of the high binding energy features in Figure 11a are amplified

compared to the experimental data in Figure 3c. The overall triple-peak structure is, however, reproduced also in the simulations.

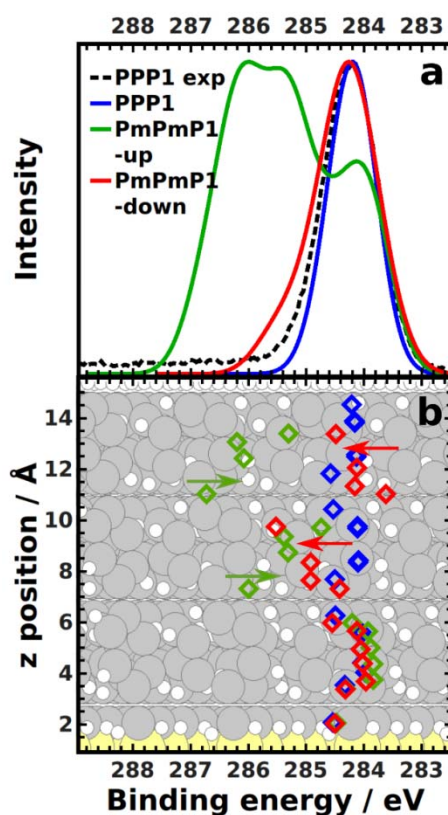


Figure 11. (a) DFT-calculated XP spectra for the PPP1 (blue), the PmPmP1-down (red) and the PmPmP1-up (green) SAMs. The spectra have been aligned to the experimental spectrum of PPP1 (dashed line) and a damping consistent with a primary photon energy of 580 eV is assumed (for details see the main text and the Supporting Information, respectively). (b) (shifted) core-level binding energies of individual C atoms averaged over equivalent atoms in the two molecules contained in the unit cell. For the spectra and the energies of the individual levels, screening effects by the substrate according to the electrostatic model described in the Supporting Information have been considered. The average positions of the N atoms in the PmPmP1-down and PmPmP1-up SAMs are indicated by red and green arrows, respectively. The z-axis is directed perpendicular to the substrate.

For PmPmP1-down, the electrostatic shifts in the simulations result in a marked reduction of the binding energies of the carbon atoms in the topmost ring. Thus, they essentially coincide with the binding energies in the PPP1 SAM, despite the chemical shifts due to bonding to the nitrogen atoms. This near compensation of chemical and electrostatic shifts for the topmost ring of PmPmP1-down results in a simulated XP spectrum that differs from that of PPP1 only by a

small shoulder at the high energy side. Compared to the experiments, the magnitude of that shoulder is strongly underestimated in the simulations, which is a consequence of the much larger shift in electrostatic energy in the calculations compared to the experiments (c.f., Fig. 11), as discussed earlier already for the work-function changes. This larger shift in the simulations is also the reason, why in Figure 11a the peak maxima for the spectra of PmPmP1-down and PPP1 coincide, while there is a shift in the peak positions in Figure 3c.

3.12. The Impact of Structural Imperfections, Depolarization, Fermi-Level Pinning, and Adsorbates

Both PmPm-up/down and PmPmP1-up/down SAMs cause a change in the work function relative to the non-polar reference SAM which is consistent with the orientation of the dipole of the pyrimidines. For several systems, the magnitude of the shift is, however, distinctly smaller than expected. For the two-ring systems (PmPm-up/down) this can be traced back to a comparably low quality of the films. In contrast, all experiments as well as the simulations imply that the three-ring PmPmP1-up/down SAMs are well ordered with molecules in a close to upright orientation. Nevertheless, especially for PmPmP1-down, the measured work-function changes are significantly smaller than expected considering the molecular structure. For this system, also the simulations suggest a much larger work-function change. In the following, possible reasons for this deviation shall be discussed.

Identity and purity of the SAM precursors. The most "simple" explanation would be a not well-defined character and slight impurities of the SAM precursors. This can, however, be fully excluded in view of the available mass-spectrometry, NMR-, and IR-spectroscopy data for all intermediate and target compounds as well as by the established handling of the compounds in the course of the synthesis procedure and the SAM preparation.

Structural imperfections. A further possible explanation for a reduced work function modification in the experiments could be structural imperfections with reduced coverage and more strongly tilted molecules, e.g., in the vicinity of domain boundaries of the SAMs. The STM, FTIR, XPS, NEXAFS spectroscopy and ellipsometry data, however, testify to an overall high film quality of the PmPmP1-up/down SAMs and an essentially upright orientation of the molecules (in contrast to PmPm-up). Moreover, there is no indication that the PmPmP1-down SAM would be less well ordered than PmPmP1-up. In fact, the structural parameters of the PmPmP1-down SAM are close to that of the PmPmP1-up, even though the packing density is somewhat lower.

The situation is different for the two-ring systems and here especially for PmPm-up. The structural quality of this SAM is inferior to all other monolayers of this study and some of the results are only poorly reproducible. Notably, for PmPm-up the thione is the dominant tautomer in the solid state and in solution, as follows from the yellow color of the neat substance (see section 3.2), similarities of its IR spectrum with the calculated IR spectrum of the thione (see section 3.8), and a new broad singlet at 14.22 ppm and a vanishing thiol peak in the corresponding ^1H NMR spectrum (see the Supporting Information). The IRRA spectrum, however, clearly shows the deposition of the thiolate form (see section 3.8). From this, we conclude that on the surface thione formation is not a problem. We rather hypothesize that in PmPm-up the close proximity of the nitrogen atoms of the "bottom" pyrimidine ring to the substrate is primarily responsible for the poor film quality.

Falsely aligned molecules. A possible scenario for a reduced work function modification would be a partial dipole compensation driven by incorporation of molecules which are flipped by 180° . This would not necessarily result in a deterioration of the structure of the films. It would, however, require some of the thiol groups to stick out of the SAM rather than to bond to the surface. Considering the different chemical environments of the S atoms in the thiolates bonded to the substrate and in the thiols sticking out of the sample, such misaligned molecules ought to be easily detectable via chemical shifts of the S 2p core levels. In this context, one, however, has to keep in mind that due to the polar groups present in the SAM, there is an electrostatic shift of the binding energies superimposed on the chemical one (vide supra). To address this issue, we did test calculation on SAMs with 25% flipped molecules (see the Supporting Information). Interestingly, for the PmPmP1-up SAM, the superposition of chemical and electrostatic shifts played out such that the calculated core level energies for the S atoms in the thiolates at the interface with the Au substrate were within 0.1 eV of the binding energies of the thiols on the SAM surface in the flipped molecules. As the electrostatic shift for the PmPmP1-down SAM goes in the opposite direction, there such a cancellation does not happen. Thus, we can also exclude misaligned molecules to be responsible for the comparably small work function modification observed for the PmPmP1-down SAM.

Depolarization effects. Depolarization effects typically cause a sub-linear increase of the work function with the molecular dipole moment, as dipoles aligned perpendicular to the plane in which they are arranged create fields that reduce each other's magnitude.⁷⁶⁻⁷⁹ This effect should, however not strongly increase with the number of pyrimidine rings, as for distributed dipole SAMs, depolarization effects primarily stem from the interaction within pyrimidine sheets due to the very short decay length of the electric field generated by ordered dipole assemblies.⁸⁰

Moreover, depolarization effects are fully accounted for in the simulations on the SAMs and, therefore, cannot explain the massive difference between the experimental data and theoretical estimates for these systems.

Fermi level pinning. When the polar groups contained in the SAM-forming molecules are strong enough to shift occupied or unoccupied states into resonance with the Fermi level of the substrate, further changes in the molecular dipole moments no longer modify the SAM-induced work function change.⁸¹ In that case, the sample work function is essentially determined by the electron affinity or ionization energy of the adsorbed monolayer.⁷ Actually, some of us predicted that Fermi level pinning would indeed limit the achievable work function change of oligopyrimidine SAMs with “down” oriented dipoles.¹⁹ Also in the present simulations, the onset of the HOMO-derived band for the PmPmP1-down SAM coincides with the Fermi level (see the Supporting Information). This pinning, however, occurs for a work function change of $\Delta\Phi = +2.39$ eV, i.e., a value much more positive than in the experiments. This value provides a lower limit to the onset of pinning, as simulations on aromatic SAMs employing (semi)local functionals usually predict a too small rather than a too large ionization energy.^{82,83} Therefore, also Fermi level pinning cannot explain the electronic properties of the PmPmP1-down SAM.

Adsorption of airborne molecules on the SAM surface. All SAMs presented in this study have been grown from solution and afterwards been handled in ambient air. Thus, one cannot exclude that contaminants adsorb on the surface of the SAMs. It is not unrealistic that such adsorbates would most strongly interact with the comparably more polar surface of the PmPmP1-down SAM, as in this system the nitrogen atoms of the pyrimidines are directly exposed at the SAM surface. This could also explain, why in the experiments (in contrast to the simulations, see the Supporting Information), the N 1s core-level binding energies shift in the opposite direction compared to the main C 1s peak, when going from PmPmP1-up to PmPmP1-down. Considering the measured N 1s binding energies for the series PmPmP1-up \rightarrow PPmP1-up \rightarrow PPmP1-down \rightarrow PmPmP1-down, namely 398.9 eV \rightarrow 398.6 eV \rightarrow 398.3 eV \rightarrow 399.3 eV (see section 3.6 and ref 13), one indeed sees that the outlier in the series is the PmPmP1-down SAM. We hypothesize that the interaction between the airborne adsorbates and the N atoms in the topmost ring of PmPmP1-down not only triggers a chemical shift of the corresponding N 1s signal but also interferes with the dipole of the top pyrimidine ring in that SAM and, thus, could diminish its impact on the work function modification and the XP spectra. A further argument in favor of such an interpretation is the O 1s XP spectrum of the PmPmP1-down SAM, which shows a noticeably stronger contribution of an oxygen-containing contaminant compared to PmPmP1-up/Au and PPP1/Au (see section 3.6). A small amount of carbon-containing adsorbates is

possible as well but is hardly traceable in the XP spectra,²⁷ unless one has a vacuum-only or contamination-free reference of the same sample.⁸⁴ This, in our opinion, leaves the ambient effect scenario as the most likely one for explaining the unexpected work function of the PmPmP1-down SAM. It also raises the question, whether such effects might occur more often than so far reported for SAMs exposing functional groups at their surface.

4. Summary and Conclusions

In the present study, we present a series of distributed-dipole SAMs on Au(111) containing 2,5'-bipyrimidine as a polar unit. The bipyrimidine was either directly attached to a thiol anchoring group (PmPm-up/down) or separated from it by a phenylene-methylene spacer (PmPmP1-up/down), decoupling the dipolar moiety from the substrate and promoting the monomolecular assembly. The SAMs were characterized by combining a large pool of analytic techniques together with dispersion-corrected DFT calculations.

The PmPm-up/down SAMs turned out to be less promising, with especially the PmPm-up monolayers exhibiting a particular low packing density and an inferior quality. This can be tentatively explained by the close proximity of the nitrogen atoms of the "bottom" pyrimidine unit to the substrate. In contrast, the PmPmP1-up/down SAMs with the decoupled bipyrimidine units are of high quality with nearly upright-standing molecules, a high packing density, close to that of non-substituted alkanethiolates, and an ordered molecular lattice with a basic $(\sqrt{3} \times \sqrt{3})R30^\circ$ motif.

Interestingly, changing the orientation of the bipyrimidine unit in the PmPmP1-up/down SAMs allows varying the substrate work function over a range of ~ 1.35 eV. Considering that SAMs with only a single embedded pyrimidine group yielded a tuning range of ~ 1.0 eV,^{13,15} this means that the effect of the additional pyrimidine group is noticeably smaller than expected. An in-depth analysis shows that for the "up" dipole orientation the work function change relative to a terphenyl-based reference SAM scales roughly linearly with the number of pyrimidine units. Conversely, the impact of the second pyrimidine ring in PmPmP1-down is negligible. A variety of factors that could be responsible for this behavior are discussed. They comprise aspects like disorder, depolarization, and Fermi level pinning, but the most likely scenario is the adsorption of minor amounts of unspecific airborne contaminants on the SAM surface during its exposure to ambient, as these adsorbates may interact with the exposed nitrogen atoms of the topmost rings in PmPmP1-down SAMs.

From a practical point of view, PmPmP1-up is especially promising, since it gives a noticeable reduction of the work function (by -0.72 eV compared to a PPP1 SAM bearing no embedded dipoles), which is distinctly larger than for the analogous monopyrimidine monolayer, PPmP1-up/Au (-0.42 eV). This makes it particularly promising for realizing n-type devices employing, e.g., Au electrodes.¹⁸ Moreover, SAM-ambient interface for PmPmP1-up is largely decoupled from the heteroatoms in the topmost ring.

Associated content

Supporting Information

The Supporting Information is available free of charge on the ACS Publication website at DOI: Exact description of the procedures for the synthesis of the SAM precursors; additional experimental data; computational details and additional modelling data (PDF). The cif files of the X-ray data of compounds **1** (CCDC 1583356), **2** (CCDC 1583357), **3** (CCDC 1953953), and the corresponding disulfide of **4** (CCDC 1953954).

Author Information

Corresponding Author

*E-mail: egbert.zojer@tugraz.at

*E-mail: aterfort@chemie.uni-frankfurt.de

*E-mail: Michael.Zharnikov@urz.uni-heidelberg.de

ORCID

Egbert Zojer: 0000-0002-6502-1721

Andreas Terfort: 0000-0003-2369-5151

Michael Zharnikov: 0000-0002-3708-7571

Martin Kind: 0000-0002-9896-9615

Author Contributions

M.G., E.S., and G.N. have provided equivalent contributions

Notes

The authors declare no competing financial interest.

Acknowledgements

E.S. and M.Z. thank the Helmholtz Zentrum Berlin for the allocation of synchrotron radiation beamtime at BESSY II and financial support as well as A. Nefedov and Ch. Wöll for the technical cooperation during the experiments there. A.A. acknowledges the financial support by the DAAD-Aceh Scholarship of Excellence. The work was financially supported by the German Research Foundation (Deutsche Forschungsgemeinschaft; DFG) via grants ZH 63/22-1 (E.S. and M.Z.) and TE247/15-1 (M.G. and A.T.) as well as by the Austrian Science Fund (FWF) via grants I2081-N20 and P28015-N36. The computational results have been in part achieved using the Vienna Scientific Cluster (VSC3). We want to thank Südchemie/Clariant for the generous donation of triisopropylsilane and pyrimidine derivatives as well as Rockwood/Albemarle for the generous donation of several alkyllithium reagents.

References

- (1) Koch, N. Energy Levels at Interfaces between Metals and Conjugated Organic Molecules. *J. Phys.: Condens. Matter* **2008**, *20*, 184008.
- (2) Liu, C.; Xu, Y.; Noh, Y.-Y. Contact Engineering in Organic Field-Effect Transistors. *Mater. Today* **2015**, *18*, 79–96.
- (3) Hamadani, B. H.; Corley, D. A.; Ciszek, J. W.; Tour, J. M.; Natelson, D. Controlling Charge Injection in Organic Field-Effect Transistors Using Self-Assembled Monolayers. *Nano Lett.* **2006**, *6*, 1303–1306.
- (4) Lange, I.; Reiter, S.; Pätzelt, M.; Zykov, A.; Nefedov, A.; Hildebrandt, J.; Hecht, S.; Kowarik, S.; Wöll, C.; Heimel, G. et al., Tuning the Work Function of Polar Zinc Oxide Surfaces using Modified Phosphonic Acid Self-Assembled Monolayers. *Adv. Funct. Mater.* **2014**, *24*, 7014–7024.
- (5) Lee, H. Ju; Jamison, A. C.; Lee, T. R. Surface Dipoles: A Growing Body of Evidence Supports Their Impact and Importance. *Acc. Chem. Res.* **2015**, *48*, 3007–3015.
- (6) Borchert, J. W.; Peng, B.; Letzkus, F.; Burghartz, J. N.; Chan, P. K. L.; Zojer, K.; Ludwigs, S.; Klauk, H. Small Contact Resistance and High-Frequency Operation of Flexible Low-Voltage Inverted Coplanar Organic Transistors. *Nat. Commun.* **2019**, *10*:1119.
- (7) Zojer, E.; Taucher, T. C.; Homann, O. T. The Impact of Dipolar Layers on the Electronic Properties of Organic/Inorganic Hybrid Interfaces, *Adv. Mater. Interf.* **2019**, 1900581.
- (8) Love, J. C.; Estroff, L. A.; Kriebel, J. K.; Nuzzo, R. G.; Whitesides, G. M. Self-Assembled Monolayers of Thiolates on Metals as a Form of Nanotechnology. *Chem. Rev.* **2005**, *105*, 1103–1169.
- (9) Alloway, D. M.; Graham, A. L.; Yang, Xi; Mudalige, A.; Colorado, Jr., R.; Wysocki, V. H.; Pemberton, J. E.; Lee, T. R.; Wysocki, R. J.; Armstrong, N. R. Tuning the Effective Work Function of Gold and Silver Using ω -Functionalized Alkanethiols: Varying Surface Composition through Dilution and Choice of Terminal Groups. *J. Phys. Chem. C* **2009**, *113*, 20328–20334.
- (10) Schmidt, C.; Witt, A.; Witte, G. Tailoring the Cu(100) Work Function by Substituted Benzenethiolate Self-Assembled Monolayers. *J. Phys. Chem. A* **2011**, *115*, 7234–7241.
- (11) Ford, W. E.; Gao, D.; Knorr, N.; Wirtz, R.; Scholz, F.; Karipidou, Z.; Ogasawara, K.; Rosselli, S.; Rodin, V.; Nelles, G.; et al. Organic Dipole Layers for Ultralow Work Function Electrodes. *ACS Nano* **2014**, *8*, 9173–9180.

(12) Kim, J.; Rim, Y. S.; Liu, Y.; Serino, A. C.; Thomas, J. C.; Chen, H.; Yang, Y.; Weiss, P. S. Interface Control in Organic Electronics Using Mixed Monolayers of Carboranethiol Isomers. *Nano Lett.* **2014**, *14*, 2946–2951.

(13) Abu-Husein, T.; Schuster, S.; Egger, D. A.; Kind, M.; Santowski, T.; Wiesner, A.; Chiechi, R.; Zojer, E.; Terfort, A.; Zharnikov, M. The Effects of Embedded Dipoles in Aromatic Self-Assembled Monolayers. *Adv. Funct. Mater.* **2015**, *25*, 3943–3957.

(14) Cabarcos, O. M.; Schuster, S.; Hehn, I.; Zhang, P. P.; Maitani, M. M.; Sullivan, N.; Giguère, J.-B.; Morin, J.-F.; Weiss, P. S.; Zojer, E.; et al. Effects of Embedded Dipole Layers on Electrostatic Properties of Alkanethiolate Self-Assembled Monolayers. *J. Phys. Chem. C* **2017**, *121*, 15815–15830.

(15) Gärtner, M.; Sauter, E.; Nascimbeni, G.; Petritz, A.; Wiesner, A.; Kind, M.; Abu-Husein, T.; Bolte, M.; Stadlober, B.; Zojer, E.; et al. Understanding the Properties of Tailor-Made Self-Assembled Monolayers with Embedded Dipole Moments for Interface Engineering. *J. Phys. Chem. C* **2018**, *122*, 28757–28774.

(16) Hehn, I.; Schuster, S.; Wächter, T.; Abu-Husein, T.; Terfort, A.; Zharnikov, M.; Zojer, E. Employing X-ray Photoelectron Spectroscopy for Determining Layer Homogeneity in Mixed Polar Self-Assembled Monolayers. *J. Phys. Chem. Lett.* **2016**, *7*, 2994–3000.

(17) Sauter, E.; Gilbert, C.-O.; Morin, J.-F.; Terfort, A.; Zharnikov, M. Mixed Monomolecular Films with Embedded Dipolar Groups on Ag(111). *J. Phys. Chem. C* **2018**, *122*, 19514–19523.

(18) Petritz, A.; Krammer, M.; Sauter, E.; Gärtner, M.; Nascimbeni, G.; Schrode, B.; Fian, A.; Gold, H.; Cojocar, A.; Karner-Petritz, E.; et al. Embedded Dipole Self-Assembled Monolayers for Contact Resistance Tuning in p- and n-Type Organic Thin Film Transistors and Flexible Electronic Circuits. *Adv. Funct. Mater.* **2018**, *28*, 1804462.

(19) Egger, D. A.; Rissner, F.; Rangger, G.; Hofmann, O. T.; Wittwer, L.; Heimel, G.; Zojer, E. Self-Assembled Monolayers of Polar Molecules on Au(111) Surfaces: Distributing the Dipoles. *Phys. Chem. Chem. Phys.*, **2010**, *12*, 4291–4294. Please note that in this reference, “up” and “down” refer to the positions of the N atoms in the pyrimidines, rather than to the dipole orientation. Thus, what is referred to as “up” in that paper, corresponds to “down” SAMs in all following papers on pyrimidine-containing SAMs and vice versa.

- (20) Morales, G. M.; Jiang, P.; Yuan, S.; Lee, Y.; Sanchez, A.; You, W.; Yu, L. Inversion of the Rectifying Effect in Diblock Molecular Diodes by Protonation, *J. Am. Chem. Soc.* **2005**, *127*, 10456-10457.
- (21) Lee, Y.; Carsten, B.; Yu, L. Understanding the Anchoring Group Effect of Molecular Diodes on Rectification, *Langmuir* **2009**, *25*, 1495–1499.
- (22) Díez-Pérez, I; Hihath, J.; Youngu, L.; Yu, L.; Adamska, L.; Kozhushner, M. A.; Oleynik, I. I.; Tao, N. Rectification and Stability of a Single Molecular Diode with Controlled Orientation, *Nat. Chem.* **2009**, *1*, 635-641.
- (23) Shaporenko, A.; Brunnbauer, M.; Terfort, A.; Grunze, M.; Zharnikov, M. Structural Forces in Self-Assembled Monolayers: Terphenyl-Substituted Alkanethiols on Noble Metal Substrates. *J. Phys. Chem. B* **2004**, *108*, 14462-14469.
- (24) Kang, J. F.; Ulman, A.; Liao, S.; Jordan, R.; Yang, G. H.; Liu, G. Y. Self-Assembled Rigid Monolayers of 4'-substituted-4-mercaptobiphenyls on Gold and Silver Surfaces. *Langmuir* **2001**, *17*, 95–106.
- (25) Ishida, T.; Mizutani, W.; Choi, N.; Akiba, U.; Fujihira, M.; Tokumoto, H. Structural Effects on Electrical Conduction of Conjugated Molecules Studied by Scanning Tunneling Microscopy. *J. Phys. Chem. B* **2000**, *104*, 11680-11688.
- (26) Zharnikov, M. High-Resolution X-Ray Photoelectron Spectroscopy in Studies of Self-Assembled Organic Monolayer. *J. Electron Spectr. Relat. Phenom.* **2010**, *178-179*, 380-393.
- (27) Sauter, E.; Yildirim, C.; Terfort, A.; Zharnikov, M. Adjustment of the Work Function of Pyridine and Pyrimidine Substituted Aromatic Self-Assembled Monolayers by Electron Irradiation. *J. Phys. Chem. C* **2017**, *121*, 12834–12841.
- (28) Frisch, M. J.; Schlegel, H. B.; Scuseria, G. E.; Robb, M. A.; Cheeseman, J. R.; Scalmani, G.; Barone, V.; Mennucci, B.; Petersson, G. A.; Nakatsuji, H.; et al. Gaussian 09, Revision A.02; Gaussian: Wallingford, CT, 2009.
- (29) Perdew, J. Density-Functional Approximation for the Correlation Energy of the Inhomogeneous Electron Gas. *Phys. Rev. B* **1986**, *33*, 8822–8824.
- (30) Becke, A. D. Density-Functional Exchange-Energy Approximation with Correct Asymptotic Behavior. *Phys. Rev. A* **1988**, *38*, 3098–3099.
- (31) Weigend, F.; Ahlrichs, R. Balanced Basis Sets of Split Valence, Triple Zeta Valence and Quadruple Zeta Valence Quality for H to Rn: Design and Assessment of Accuracy. *Phys. Chem. Chem. Phys.* **2005**, *7*, 3297–3305.
- (32) Nefedov, A.; Wöll, C. Advanced Applications of NEXAFS Spectroscopy for Functionalized Surfaces, in *Surface Science Techniques*; Bracco, G.; Holst, B., Eds.; Springer

Series in Surface Science **2013**, *51*, 277-306; Springer-Verlag, Berlin, Heidelberg, New York, Tokyo.

(33) Moulder, J. F.; Stickle, W. E.; Sobol, P. E.; Bomben, K. D. In *Handbook of X-ray Photoelectron Spectroscopy*, Chastian, J., Ed.; Perkin-Elmer Corp.: Eden Prairie, MN, 1992.

(34) Schreiber, F. Structure and Growth of Self-Assembled Monolayers. *Prog. Surf. Sci.* **2000**, *65*, 151–256.

(35) Stöhr, J. *NEXAFS Spectroscopy*; Springer-Verlag: Berlin, 1992.

(36) Batson, P. E. Carbon-1s Near-Edge-Absorption Fine-Structure in Graphite. *Phys. Rev. B* **1993**, *48*, 2608-2610.

(37) Blum, V.; Gehrke, R.; Hanke, F.; Havu, P.; Havu, V.; Ren, X.; Reuter, K.; Scheffler, M. Ab Initio Molecular Simulations with Numeric Atom-Centered Orbitals. *Comput. Phys. Commun.* **2009**, *180*, 2175–2196.

(38) Perdew, J.; Burke, K.; Ernzerhof, M. Generalized Gradient Approximation Made Simple, *Phys. Rev. Lett.* **1996**, *77*, 3865-3868.

(39) Ruiz, V. G.; Liu, W.; Zojer, E.; Scheffler, M.; Tkatchenko, A. Density-Functional Theory with Screened van der Waals Interactions for the Modeling of Hybrid Inorganic-Organic Systems. *Phys. Rev. Lett.* **2012**, *108*, 146103.

(40) Tkatchenko, A.; Scheffler, M. Accurate Molecular van der Waals Interactions from Ground-State Electron Density and Free-Atom Reference Data. *Phys. Rev. Lett.* **2009**, *102*, 073005.

(41) Freysoldt, C.; Eggert, P.; Rinke, P.; Schindlmayr, A.; Scheffler, M. Screening in Two Dimensions: GW Calculations for Surfaces and Thin Films Using the Repeated-Slab Approach. *Phys. Rev. B.* **2008**, *77*, 235428.

(42) Taucher, T. C.; Hehn, I.; Hofmann, O. T.; Zharnikov, M.; Zojer, E. Understanding Chemical versus Electrostatic Shifts in X-Ray Photoelectron Spectra of Organic Self-Assembled Monolayers. *J. Phys. Chem. C* **2016**, *120*, 3428–3437.

(43) Levstik, A.; Filipič, C.; Levstik, I. Dielectric properties of Biphenyl. *J. Phys.: Condens. Matter* **1990**, *2*, 3031–3033.

(44) Foye, W. O.; Abood, N.; Kauffman, J. M.; Kim, Y.-H.; Patel, B. R. A Direct Synthesis of Heterocyclic Thiols, *Phosphorous Sulfur Relat. Elem.* **1980**, *8*, 205–207.

(45) Schüpbach, B.; Terfort, A. A Divergent Synthesis of Oligoarylalkanethiols with Lewis-Basic N-Donor Termini. *Org. Biomol. Chem.* **2010**, *8*, 3552-3562.

(46) Kondoh, H.; Iwasaki, M.; Shimada, T.; Amemiya, K.; Yokoyama, T.; Ohta, T.; Shimomura, M.; Kono, S. Adsorption of Thiolates to Singly Coordinated Sites on Au(111) Evidenced by Photoelectron Diffraction. *Phys. Rev. Lett.* **2003**, *90*, 066102.

(47) Roper, M. G.; Skegg, M. P.; Fisher, C. J.; Lee, J. J.; Dhanak, V. R.; Woodruff, D. P.; Jones, R. G. Atop Adsorption Site of Sulphur Head Groups in Gold-Thiolate Self-Assembled Monolayers. *Chem. Phys. Lett.* **2004**, *389*, 87-91.

(48) Ishida, T.; Mizutani, W.; Akiba, U.; Umemura, K.; Inoue, A.; Choi, N.; Fujihira, M.; Tokumoto, H. Lateral Electrical Conduction in Organic Monolayer. *J. Phys. Chem. B* **1999**, *103*, 10, 1686-1690.

(49) Leung, T. Y. B.; Schwartz, P.; Scoles, G.; Schreiber, F.; Ulman, A. Structure and Growth of 4-Methyl-4'-Mercaptobiphenylmonolayers on Au(111): a Surface Diffraction Study. *Surf. Sci.* **2000**, *458*, 34-52.

(50) Ishida, T.; Mizutani, W.; Azebara, H.; Sato, F.; Choi, N.; Akiba, U.; Fujihira, M.; Tokumoto, H. Adsorption Processes of Self-Assembled Monolayers Made from Terphenyl Thiols, *Langmuir* **2001**, *17*, 7459-7463.

(51) Azzam, W.; Fuxen, C.; Birkner, A.; Rong, H.-T.; Buck, M.; Wöll, C. Coexistence of Different Structural Phases in Thioaromatic Monolayers on Au(111). *Langmuir* **2003**, *19*, 4958-4968.

(52) Azzam, W.; Cyganik, P.; Witte, G.; Buck, M.; Wöll, Ch. Pronounced Odd-Even Changes in the Molecular Arrangement and Packing Density of Biphenyl-Based Thiol SAMs: A Combined STM and LEED Study. *Langmuir* **2003**, *19*, 8262-8270.

(53) Azzam, W.; Bashir, A.; Terfort, A.; Wöll, Ch. Combined STM and FTIR Characterization of Terphenylalkanethiol Monolayers on Au(111): Effect of Alkyl Chain Length and Deposition Temperature. *Langmuir* **2006**, *22*, 3647-3655.

(54) Bashir, A.; Azzam, W.; Rohwerder, M.; Terfort, A. Polymorphism in Self-Assembled Terphenylthiolate Monolayers on Au(111). *Langmuir* **2013**, *29*, 13449-13456.

(55) Fuxen, C.; Azzam, W.; Arnold, R.; Witte, G.; Terfort, A.; Wöll, C. Structural Characterization of Organothiolate Adlayers on Gold: The Case of Rigid, Aromatic Backbones. *Langmuir* **2001**, *17*, 3689-3695.

(56) Ratner, M.; Castner, D. Electron Spectroscopy for Chemical Analysis, In *Surface Analysis - The principal techniques*; Vickerman, J. Ed.; Wiley: Chichester, 1997.

(57) Shaporenko, A.; Elbing, M.; Błaszczuk, A.; von Hänisch, C.; Mayor, M.; Zharnikov, M. Self-Assembled Monolayers from Biphenyldithiol Derivatives: Optimization of the

Deprotection Procedure and Effect of the Molecular Conformation. *J. Phys. Chem. B* **2006**, *110*, 4307-4317.

(58) Bolognesi, P.; O’Keeffe, P.; Feyer, V.; Plekan, O.; Prince, K.; Coreno, M.; Mattioli, G.; Amore Bonapasta, A.; Zhang, W.; Carravetta, V.; et al. Inner Shell Excitation, Ionization and Fragmentation of Pyrimidine. *J. Phys.: Conf. Ser.* **2010**, *212*, 012002.

(59) Gelius, U.; Hedman, P. F.; Hedman, J.; Lindberg, B. J.; Marine, R.; Nordberg, R.; Nordling, C.; Siegbahn, K. Molecular Spectroscopy by Means of ESCA III. Carbon Compounds. *Phys. Scr.* **1970**, *2*, 70-80.

(60) Zubavichus, Y.; Zharnikov, M.; Yang, Y.-J.; Fuchs, O.; Heske, C.; Umbach, E.; Ulman, A.; Grunze, M. XPS and NEXAFS Study of Water Adsorption on the Pyridine-Terminated Thiolate Self-Assembled Monolayer. *Langmuir* **2004**, *20*, 11022-11029.

(61) Mille, G.; Guilano, M.; Kister, J.; Chouteau, J.; Metzger, J. Analyse des Spectres de Vibration des Alkyl(Allyl, Benzyl) Thio-2-Pyrimidines. *Spectrochim. Acta A* **1980**, *36*, 713-720.

(62) Sathyanarayana, D. N.; Kasmir Raja, S. V. Molecular Vibrations of Pyridine-2-Thione and Pyrimidine-2-Thione. *Spectrochim. Acta A* **1985**, *41*, 809-813.

(63) Greenler, R. G. Infrared Study of Adsorbed Molecules on Metal Surfaces by Reflection Techniques. *J. Chem. Phys.* **1966**, *44*, 310–315.

(64) Parikh, A. N.; Allara, D. L. Quantitative Determination of Molecular Structure in Multilayered Thin Films of Biaxial and Lower Symmetry from Photon Spectroscopies. I. Reflection Infrared Vibrational Spectroscopy. *J. Chem. Phys.* **1992**, *96*, 927–945.

(65) Horsley, J.; Stöhr, J.; Hitchcock, A. P.; Newbury, D. C.; Johnson, A. L.; Sette, F. Resonances in the *K* Shell Excitation Spectra of Benzene and Pyridine: Gas Phase, Solid, and Chemisorbed States. *J. Chem. Phys.* **1985**, *83*, 6099-6107.

(66) Yokoyama, T.; Seki, K.; Morisada, I.; Edamatsu, K.; Ohta, T. X-Ray Absorption Spectra of Poly-p-Phenylenes and Polyacenes: Localization of π^* Orbitals. *Phys. Scr.* **1990**, *41*, 189-192.

(67) Frey, S.; Stadler, V.; Heister, K.; Eck, W.; Zharnikov, M.; Grunze, M.; Zeysing, B.; Terfort, A. Structure of Thioaromatic Self-Assembled Monolayers on Gold and Silver. *Langmuir* **2001**, *17*, 2408-2415.

(68) Bolognesi, P.; O’Keeffe, P.; Ovcharenko, Y.; Coreno, M.; Avaldi, L.; Feyer, V.; Plekan, O.; Prince, K. C.; Zhang, W.; Carravetta, V. Pyrimidine and Halogenated Pyrimidines Near Edge X-ray Absorption Fine Structure Spectra at C and N K-Edges: Experiment and Theory. *J. Chem. Phys.* **2010**, *133*, 034302.

- (69) Lin, Yi-S.; Lin, H.-Ru; Liu, W.-L.; Lee, Y. T.; Tseng, C.-M.; Ni, C.-K.; Liu, C.-L.; Tsai, C.-C.; Chen, J.-L.; Hu, W.-P. Measurement and Prediction of the NEXAFS Spectra of Pyrimidine and Purine and the Dissociation Following the Core Excitation. *Chem. Phys. Lett.* **2015**, *636*, 146-153.
- (70) Ballav, N.; Schüpbach, B.; Dethloff, O.; Feulner, P.; Terfort, A.; Zharnikov, M. Direct Probing Molecular Twist and Tilt in Aromatic Self-Assembled Monolayers. *J. Am. Chem. Soc.* **2007**, *129*, 15416–15417.
- (71) Vackář, J.; Hyt'ha, M.; Šimůnek, A. All-Electron Pseudopotentials. *Phys. Rev. B* **1998**, *58*, 12712–12720.
- (72) Morikawa, Y.; Hayashi, T.; Liew, C. C.; Nozoye, H. First-Principles Theoretical Study of Alkylthiolate Adsorption on Au(111). *Surf. Sci.* **2002**, *507*, 46–50.
- (73) Heimel, G.; Romaner, L.; Brédas, J.-L.; Zojer, E. Organic/Metal Interfaces in Self-Assembled Monolayers of Conjugated Thiols: A First-Principles Benchmark Study. *Surf. Sci.* **2006**, *600*, 4548-4562.
- (74) Giesbers, M.; Marcelis, A. T. M.; Zuilhof, H. Simulation of XPS C1s Spectra of Organic Monolayers by Quantum Chemical Methods. *Langmuir* **2013**, *29*, 4782-4788.
- (75) Ishiwari, F.; Nascimbeni, G.; Sauter, E.; Tago, H.; Shoji, Y.; Fujii, S.; Kiguchi, M.; Tada, T.; Zharnikov, M.; Zojer, E.; et al. Triptycene Tripods for the Formation of Highly Uniform and Densely Packed Self-Assembled Monolayers with Controlled Molecular Orientation. *J. Am. Chem. Soc.* **2019**, *141*, 5995–6005.
- (76) Natan, A. ; Zidon, Y. ; Shapira, Y.; Kronik, L. Cooperative Effects and Dipole Formation at Semiconductor and Self-Assembled-Monolayer Interfaces, *Phys. Rev. B* **2006**, *73*, 193310.
- (77) Blumenfeld, M. L.; Steele, M. P.; Monti, O. L. A. Near- and Far-Field Effects on Molecular Energy Level Alignment at an Organic/Electrode Interface, *J. Phys. Chem. Lett.* **2010**, *1*, 145–148.
- (78) Cornil, D.; Olivier, Y.; Geskin, V.; and Cornil, J., Depolarization Effects in Self-Assembled Monolayers: A Quantum-Chemical Insight, *Adv. Funct. Mater.* **2007**, *17*, 1143–1150.
- (79) Romaner, L.; Heimel, G.; Ambrosch-Draxl, C.; Zojer, E. The Dielectric Constant of Self-Assembled Monolayers, *Adv. Funct. Mater.* **2008**, *18*, 3999-4006; **2011**, *21*, 3406 (Erratum).

(80) Natan, A.; Kronik, L.; Haick, H.; Tung, R. T. Electrostatic Properties of Ideal and Non-ideal Polar Organic Monolayers: Implications for Electronic Devices. *Adv. Mater.* **2007**, *19*, 4103–4117.

(81) Hofmann, O. T.; Egger, D. A.; Zojer, E. Work-Function Modification beyond Pinning: When Do Molecular Dipoles Count? *Nano Lett.* **2010**, *11*, 4369–4374.

(82) Track, A. M.; Rissner, F.; Heimel, G.; Romaner, L.; Käfer, D.; Bashir, A.; Rangger, G. M.; Hofmann, O. T.; Bučko, T.; Witte, G.; et al. Simultaneously Understanding the Geometric and Electronic Structure of Anthraceneselenolate on Au(111): A Combined Theoretical and Experimental Study. *J. Phys. Chem. C* **2010**, *114*, 2677–2684.

(83) Egger, D. A.; Liu, Z.-F.; Neaton, J. B.; Kronik, L. *Nano Lett.* **2015**, *15*, 2448–2455.

(84) Chen, C.-H.; Huang, M.-L.; Wang, S.-C.; Klauser, R.; Shaporenko, A.; Zharnikov, M. Exposure of Monomolecular Lithographic Patterns to Ambient: An X-ray Photoemission Spectromicroscopy Study. *J. Phys. Chem. B* **2006**, *110*, 17878–17883.

TOC graphic

